Korean J. Chem. Eng., 35(11), 2241-2255 (2018)
DOI: 10.1007/s11814-018-0038-4

pISSN: 0256-1115
eISSN: 1975-7220

Optimization and modification of PVDF dual-layer hollow fiber membrane for direct contact membrane distillation; application of response surface methodology and morphology study

Mehdi Bahrami*, Javad Karimi-Sabet,†, Ali Hatamnejad*, Abolfazl Dastbaz*, and Mohammad Ali Moosavian***

*Department of Chemical Engineering, Faculty of Engineering, University of Tehran, Tehran, Iran
**Material and Nuclear Fuel Research School (MNFRS), Nuclear Science and Technology Research Institute, Tehran, Iran
(*Received 7 October 2017 • accepted 23 February 2018*)

Abstract−RSM methodology was applied to present mathematical models for the fabrication of polyvinylidene fluoride (PVDF) dual-layer hollow fibers in membrane distillation process. The design of experiments was used to investigate three main parameters in terms of polymer concentration in both outer and inner layers and the flow rate of dope solutions by the Box-Behnken method. According to obtained results, the optimization was done to present the proper membrane with desirable properties. The characteristics of the optimized membrane (named HF-O) suggested by the Box-Behnken (at the predicted point) showed that the proposed models are strongly valid. Then, a morphology study was done to modify the fiber by a combination of three types of a structure such as macro-void, sponge-like and sharp finger-like. It also improved the hydrophobicity of outer surface from 87 to 113° and the mean pore size of the inner surface from 108.12 to 560.14 nm. The DCMD flux of modified fiber (named HF-M) enhanced 62% more than HF-O when it was fabricated by considering both of RSM and morphology study results. Finally, HF-M was conducted for long-term desalination process up to 100 hr and showed stable flux and wetting resistance during the test. These stepwise approaches are proposed to easily predict the main properties of PVDF dual-layer hollow fibers by valid models and to effectively modify its structure.

Keywords: Dual-layer Hollow Fiber Membranes, Polyvinylidene Fluoride (PVDF), Response Surface Methodology, Morphology Study, Membrane Distillation

INTRODUCTION

Industrialization and population growth have intensified the water crisis as a global issue [1,2]. Researchers have tried to find efficient desalination to overcome this problem by producing fresh water. Among the various technologies, membrane distillation (MD) has received greater attention than other conventional desalination processes like multi-stage flash distillation (MSFD) and reverse osmosis (RO), in last decays [3,4]. This is because MD process offers various advantages such as lower operating pressure and temperature, yielding highly purified distillate (theoretically 100% rejection), using natural energy sources (waste heat source, solar and geothermal energy) for operation and more cost-effective than other technologies [5,6]. Although MD is an efficient approach, it has not been industrialized yet, owing to low permeation flux and membrane pore wetting during a long-term operation [7-9]. In fact, MD is a thermally driven separation process in which the heat and mass transfer occur simultaneously and the difference of vapor pressure (temperatures) is known as the driving force between two sides of the membrane. A hydrophobic, porous membrane acting as a physical barrier between two phases is faced with a hot saline solution (feed stream) and prevents from a liquid penetration. Hence, only the vapor can diffuse into the membrane pores and migrate from the feed side. MD configurations are classified based on the methods of penetrated vapors which are condensed at distilled side. Thus, MD is divided into four distinct types: direct contact membrane distillation (DCMD), air gap membrane distillation (AGMD), vacuum membrane distillation (VMD) and sweeping gas membrane distillation (SGMD) [10-15]. Among these, DCMD is the most conventional type of MD in the literature due to more simple equipment requirement than the others and higher permeation flux. In the DCMD process, the cold pure product is applied to condense the vapors at permeate (distilled) side. Therefore, both surfaces of the membrane are directly faced with liquid streams, hot feed brine and cold pure water [16-20].

In recent years, the characteristics of MD membrane have been studied improve both permeation flux and wetting resistance. The permeation flux can be enhanced by lowering the thermal conductivity of a membrane, which results in a reduction of temperature polarization on membrane surfaces and keeping the temperature difference constant between two sides. Moreover, the mass transfer coefficient must be as high as possible to increase the diffusion rate of vapor through the membrane [21]. A membrane with large mean pore size, high porosity, low tortuosity and small thickness of the functional layer is desirable for these features (low thermal conductivity and mass transfer resistance), and its structure tends to become macro-void [22]. Note that when the thickness of the membrane is small, the amount of heat loss during the DCMD

†To whom correspondence should be addressed.
E-mail: j_karimi@alum.sharif.edu

process becomes high due to the heat conduction through the membrane matrix. On the other hand, to reduce the risk of pore wetting, high hydrophobicity, small pore size and tortuosity of the membrane are required properties for MD process [23,24]. In addition, a sponge-like structure is favorable for high wetting resistance and may improve the mechanical properties of the membrane, as well [25]. Thus, by taking into consideration both high permeation flux and wetting resistance, the desired properties of the membrane in MD are as follows: high porosity and hydrophobicity, appropriate mean pore size, optimum thickness, low thermal conductivity and combination of mentioned structure [21,26-29].

Generally, hollow fiber membranes are known as the most acceptable membrane geometry in the industrial applications due to yielding high productivity per unit volume, good flexibility in operation, mechanical self-supporting and easy assembling into the modules [30-34]. Furthermore, hollow fiber module provides the least temperature polarization than the other module configurations [10]. In MD applications, the most popular technique applied for the fabrication of hollow fiber membranes is dry/wet phase inversion spinning using poly (vinylidene fluoride) (PVDF) polymer [35,36].

The dual-layer hollow fiber membrane in MD was first proposed by Bonyadi and Chung [37] using co-extrusion technique. They fabricated hydrophobic/hydrophilic hollow fibers with the utilization of PVDF as the main polymer in both layers. They could enhance the permeation flux as high as 55 kg m^{-2} hr^{-1} at the feed inlet temperature of 90 °C in the DCMD process. A novel method for the fabrication of hydrophobic/hydrophilic composite membranes in MD was introduced by Khayet and Matsuura [27] for flat-sheet membranes as a possible method to improve the permeation flux. In the same way, many researchers employed similar approaches to fabricate hydrophobic/hydrophilic dual-layer hollow fiber membranes in MD [38-44]. Teoh and Chung [25] produced dual-layer PVDF/PTFE composite hollow fibers with a thin (13 μm) macro-void-free outer layer structure and a high wetting resistance. Wang et al. [21] offered a new structure hollow fiber consist of the sponge-like outer layer and fully finger-like macro-void inner layer. They reached a significant permeation flux as high as 98.6 Lit m^{-2} hr^{-1}.

The fabrication of hollow fiber membranes, especially dual-layer, is more complex owing to involve various parameters and interactions during the spinning process [45]. The investigation of all parameters is almost impossible by the classical method. These limitations can be avoided by using the proper design of experiment (DoE), which can investigate many variables and their interactions at the same time. The number of tests is effectively reduced rather than the conventional methods which are on the basis of trial and error [46,47]. Although some works are devoted to investigating the MD processes, limited researchers have studied it by DoE [48-50].

In this study, the fabrication of dual-layer hollow fiber membranes was modeled and studied by response surface methodology (RSM) for the first time. Three main parameters in the spinning process were investigated with four relative responses. The significant and valid models (quadratic models) were designed by Box-Behnken method based on experimental data for prediction of responses via actual terms of parameters. In addition, the parameters were optimized by consideration of the proper region of responses. Then, the morphology of inner and outer layer of the membrane was studied by altering the internal and external coagulant compositions, respectively. Finally, two resultant fibers in each part were conducted for DCMD tests and the best one of them was applied in the continuous desalination process.

EXPERIMENTAL SECTION

1. Materials and Methods

1-1. Materials

The polymer polyvinylidene fluoride (PVDF, Kynar MG 15) in powder form was purchased from Arkema Inc. The solvent N-Methyl-2-Pyrrolidone (NMP, >99.5%) and non-solvent Ethylene Glycol (EG, >99.5%) were supplied by Merck Co. Methanol (MeOH, >99.5%) was employed as external coagulation and Ethanol (EtOH, 99.5%) was employed for solvent exchange after spinning prepared from Merck Co, as well. Double-distilled water was purified with a deionizer resin in our laboratory and it was used in DCMD tests, external coagulation and bore fluid mixture.

1-2. Dope Preparation

In this work, PVDF has been considered as the main polymer in the inner and outer dope solutions. First, the polymer was dried in an oven at 70 °C at least for three days to remove excess moisture. To prepare the dope solutions, the polymer, and solvent or solvent/non-solvent mixture were mixed and kept stirred at approximately 40 °C during 24 hr until becoming homogeneous and transparent. Finally, the dope solutions were degassed at room temperature over a period of 6 hr and made ready to use in the spinning process.

1-3. Fiber Spinning

The hollow fiber membranes were prepared by dry/wet phase inversion process using the spinning system, which is schematically illustrated in Fig. 1. A detailed description of the spinning process and the apparatus pictures can be found in supplementary data (part S1). The fibers were post-treated by non-solvent exchange using ethanol for 4 hr to improve membrane wettability, prevent pore collapse and minimize the membrane shrinkage by reducing the surface tension [51]. Finally, the membranes were dried at ambient temperature for two days.

2. Membrane Characterization

2-1. Morphology Study

SEM pictures were taken to observe the surfaces, cross-sections and the dimensions of the membranes using scanning electron microscope (SEM, Model: AIS2100, SERON Co., Korea). The hol-

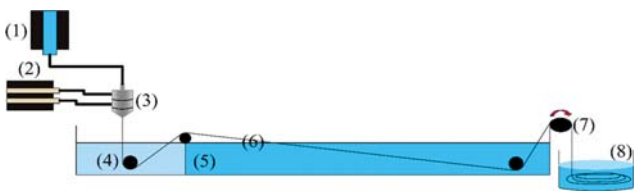

Fig. 1. Schematic diagram of the hollow fiber spinning system.

(1) Bore fluid pump
(2) Polymers pump
(3) Triple orifice spinneret
(4) External coagulant bath
(5) Water bath
(6) Nascent hollow fiber
(7) Collector
(8) Collector bath

low fiber samples were first immersed and frozen in liquid nitrogen and then fractured. The samples were subsequently subjected on a metal holder to sputter-coat with a thin gold film under vacuum.

2-2. Porosity Measurement

The overall porosity of the hollow fibers (ε) estimated by calculating the ratio of the empty voids to the total volume of the membrane was examined by kerosene immersion method [37]. First, the samples were weighted with a beam balance (w_1) and then immersed in kerosene solution for one week to ensure that all of the fiber voids were wetted and filled with kerosene, completely. Next, the wetted samples were removed from the kerosene in both lumen and surface side of fibers and subsequently weighted again (w_2). Finally, the porosity of hollow fibers was calculated by the following equation:

$$\varepsilon = \frac{w_2 - w_1}{\pi L(R_2^2 - R_1^2)\rho_{ker}} \quad (1)$$

where ε is the overall porosity, R_1 and R_2 are the inner and the outer fiber radius, respectively (obtained by SEM pictures), L is the fiber length (about 2 cm for each sample) and ρ_{ker} is the density of kerosene. An average of five measurements was considered as the fiber porosity for each sample.

2-3. Contact Angle Measurements

The contact angle of the hollow fibers was measured using a contact angle tensiometer (Model: OCA40, Data Physics Crop., Germany) with deionized water droplets to evaluate the surface hydrophobicity of the membranes. A droplet of 2 μL was leisurely put on the fiber surface and the contact angle was calculated by the software. Ten measurements in different spots of the fibers were made for samples and an average was adopted.

2-4. LEP_w, Mean Pore Size and Mechanical Strength Measurements

Liquid entry pressure of water (LEP_w, bar), mean pore size (d_p, μm) by gas permeation method and mechanical properties of membranes in terms of Young's modulus (MPa), tensile stress at break (MPa) and strain at break (%) were also applied to characterize the hollow fibers. The detailed discussion, schematic figures and the procedure of characterizations are explained in supplementary data (part S2).

3. DCMD Experiments

A lab-scale unit schematically shown in Fig. 2 was conducted for DCMD tests. The apparatus of the feed and the permeate cycles is highlighted by red and blue colors, respectively. To simulate the sea water salinity, a saline solution with 3.5 wt% sodium chloride (NaCl) concentration was used as the feed solution. The feed was heated by means of a heater and then circulated through the shell side of the membrane module. On the other hand, the distilled water was made cold by a cooler and also flowed through the lumen side of the module, which was vertically fixed on the MD installation. This was done to omit the free convection effect and remove the excess air bubbles that remained in the streams [36]. Both of the streams were pumped by peristaltic pumps and flowed co-currently through the module from the bottom to the top in order to prevent the membrane wetting generated due to the pressure difference across the opposite side of the membrane [26]. The hollow fiber modules (a plastic tube of 3/8 in. diameter) used in this experiments contain six fibers with effective length of 15 cm, packing fraction of 25±5% and filtration area about 50 cm^2. The procedure of module preparing can be found in supplementary data (part S3). The inlet temperature of the distilled water was fixed at 20 °C, while the inlet temperature of the feed solution was varied from 50 °C to 80 °C. First, the cold stream was flowed through the lumen side of the membrane module for ten minutes to ensure that there was no leakage and then the feed flowed until the steady state conditions (respective inlet temperatures and stream flow rates) were attained. For each test, the weight gain on the distilled side was measured over a predetermined period and the permeation flux, J (kg m^{-2} hr^{-1}) was calculated from the following equation:

$$J = \frac{\Delta W}{At} \quad (2)$$

where ΔW (kg) is the permeation weight change over a period of predetermined time t (hr) and A (m^2) is the effective membrane area for vapor transport. The ionic conductivity of permeate and feed solutions were measured by a conductivity meter (Model: HQ40, Hach Co., United States) and the separation factor (R) was calculated using the following expression:

$$R = \left(1 - \frac{C_P}{C_F}\right) \times 100 \quad (3)$$

where C_P and C_F are the NaCl concentration in permeate and the feed solutions, respectively.

4. Design of Experiments

Response surface method (RSM) consisting of statistical and mathematical methods has great advantages in experimental stud-

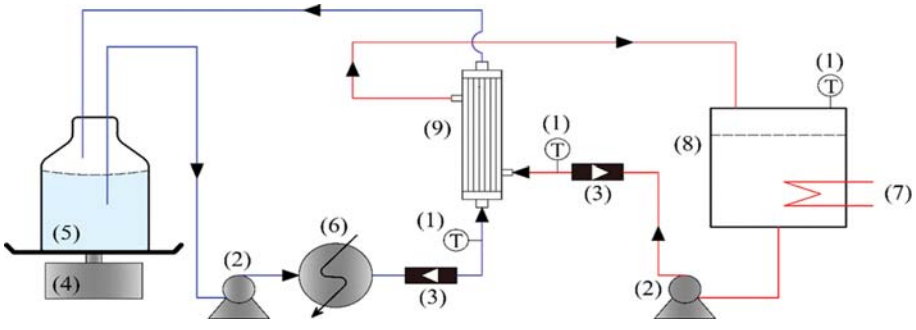

Fig. 2. Lab-scale set-up for DCMD experiment.

(1) Thermostat (2) Peristaltic pump (3) Flow meter (4) Beam balance (5) Permeate (6) Cooler (7) Heater (8) Feed (9) Hollow fiber module

Table 1. Parameters in DoE tests

Factors	Unit	Symbols	Coded and actual levels		
			Low (−1)	Center (0)	High (+1)
Outer layer polymer concentration	wt%	X_1	10	12.5	15
Inner layer polymer concentration	wt%	X_2	7	8.5	10
Dope solutions flow rate	ml/min	X_3	0.5	2.25	4

ies. The main advantages of this method are comprehensively discussed in the previous studies [52,53]. There are many parameters affecting the fabrication of the hollow fiber membrane. We applied the Box-Behnken method to design the experiments and identify the effect of three main parameters in terms of polymer concentration (wt%) in both outer and inner layer and dope solutions flow rate (ml/min). They were investigated based on four main responses such as overall porosity (ε), contact angle outer layer (°), membrane thickness (μm) and outer layer thickness (μm). These main variables and responses are chosen because (1) The polymer concentration in both inner and outer layer is one of the most significant parameters which affect the properties of the fibers. (2) The flow rate of dope solutions plays a very important role in the fabrication of fibers by inducing and altering the shear stress in the spinneret which results in affecting some properties of the fiber. (3) These responses are the most relative properties of hollow fibers, based on the selected parameters. This approach was made to obtain an appropriate membrane by the Box-Behnken method. The effects of the main parameters on the responses can be illustrated by plots and investigated via empirical models (mathematical equations). The range of the factors (parameters) concerning coded and uncoded symbols is shown in Table 1.

The relation of coded and actual values was obtained by the following equation:

$$x_i = \frac{X_i - X_0}{\Delta X_i} \quad (4)$$

where x_i and X_i are the coded and actual values of the independent variable, respectively, X_0 is the actual value of the independent variable at the center point and ΔX_i is the step change of X_i. To fit the experimental data, Eq. (5) is used by the second order polynomial model.

$$Y = \beta_0 + \Sigma_{i=1}^{k}\beta_i x_i + \Sigma_{i=1}^{k}\beta_{ii} k_i^2 + \Sigma_{1\le i<j}^{k}\beta_{ij} x_i x_j + \xi \quad (5)$$

where Y is the predicted response, x_i is the input factors, k is the number of variables, β_0 is the constant term, β_i is the linear parameters coefficient, β_{ii} and β_{ij} are the coefficient of quadratic and interaction parameters, respectively. In addition, ξ is the residual associated to the experiments [54,55]. We designed 15 experiments (including three replicative tests at the central point) by Design Expert Software (Version 10.0.2, State-Ease Inc., Minneapolis, USA). The analysis of variance (ANOVA) technique was applied to verify the statistically significant factors and interactions by probability P-value. The determination coefficient (R^2) was used to evaluate the validity of the regression model [56]. The conditions of the dual-layer hollow fiber fabrication applied for experimental design tests are summarized in Table 2. The composition of polymer (PVDF) and solvent (NMP) in the inner and outer layer solution was obtained from the Box-Behnken method. The same flow rate was considered for both inner and outer dope solutions.

Table 2. Spinning condition of dual-layer hollow fiber in experimental design tests

Bore fluid (wt%)	DI water (37.5 °C)
Bore flow rate (ml/min)	6
External coagulant (wt%)	DI water (25 °C)
Air gap (cm)	2
Take-up speed	Free fall

RESULT AND DISCUSSION

1. Response Surface Methodology

1-1. Mathematical Method of Box-Behnken

Table 3 demonstrates 15 experiments designed by the Box-Behnken method. These tests were performed to investigate the effects of the polymer concentration in the outer layer (x_1), the polymer concentration in the inner layer (x_2) and the flow rate of the dope solutions (x_3). Moreover, their corresponding responses in terms of porosity (y_1), surface hydrophobicity or contact angle (y_2), overall membrane thickness (y_3) and outer layer thickness (y_4) are studied in the present work. The analysis of variance (ANOVA) was used to examine the significance of the models and coefficients distinguished by P-value. Note that whenever the P-value gets less, the effect of coefficients terms becomes more and the validity of the model increases. P-value less than 0.05 indicates that the model and coefficient terms are statistically significant, whereas they are not valid for the model when this value is more than 0.1 [56]. ANOVA results for the quadratic model including P-values and coefficients estimate in terms of coded factors are tabulated in Table 4. By taking into consideration of the P-values less than 0.05, only some coefficients are acceptable and some of them are found to be negligible (P-values more than 0.1) for predicted responses. Based on this assumption, x_1, x_2, x_3, x_1x_3 and x_3^2 for y_1, x_1, x_3, x^{12} and x_3^2 for y_2, x_1, x_2 and x_3 for y_3 and x_1, x_3 and x_1x_2 for y_4 are the significant model terms, respectively.

Predicting the characteristics of hollow fibers applied in the MD based on the standard models is essential for the development of desalination process. Table 5 presents the empirical models in terms of actual factors, which can be used to make predictions about the respective responses. The input data for these equations should be specified in the original units for each factor. As can be observed in Table 4 and Table 5, the values of coefficient terms in the models are highly affected by the amount of p-value. As the p-value

Table 3. Box-Behnken design experiments with obtained results

Exp no.	Outer layer concentration (O, wt%)	Inner layer concentration (I, wt%)	Dopes flow rate (F, ml/min)	Porosity (ε, %)	Contact angel (θ, °)	Fiber thickness (T, μm)	Outer layer thickness (ST, μm)
1	10.00	8.50	4.00	77.79	82.25	161.028	68.385
2	12.50	7.00	0.50	88.50	80.00	25.282	10.481
3	12.50	7.00	4.00	78.50	83.00	172.736	66.776
4	12.50	10.00	0.50	74.23	80.00	44.095	17.536
5	15.00	10.00	2.25	66.85	93.00	150.711	55.512
6	10.00	8.50	0.50	82.00	79.00	23.719	9.894
7	12.50	10.00	4.00	71.50	83.25	198.330	76.374
8	12.50	8.50	2.25	70.21	83.00	108.972	42.864
9	10.00	10.00	2.25	69.98	83.50	94.819	32.557
10	15.00	8.50	0.50	79.00	86.50	34.343	13.879
11	10.00	7.00	2.25	82.87	82.75	91.154	46.183
12	12.50	8.50	2.25	73.23	85.00	95.061	39.648
13	15.00	8.50	4.00	64.00	87.00	170.679	75.005
14	15.00	7.00	2.25	76.10	91.50	89.219	43.332
15	12.50	8.50	2.25	73.11	82.25	104.734	41.275

Table 4. Analysis of variance (ANOVA) results for response surface quadratic model

Source	Porosity		Contact angle		Fiber thickness		Outer layer thickness	
	Coefficient estimate	P-value	Coefficient estimate	P-value	Coefficient estimate	P-value	Coefficient estimate	P-value
Intercept	72.18		84.42		102.92		41.26	
x_1	−3.34	0.0038	3.81	0.0002	11.90	0.0256	3.84	0.0258
x_2	−5.43	0.0004	0.31	0.4675	11.07	0.0329	1.90	0.1810
x_3	−3.99	0.0017	1.25	0.0256	71.92	<0.0001	29.34	<0.0001
x_1x_2	0.91	0.3706	0.19	0.7523	9.21	0.1463	6.45	0.0136
x_1x_3	−2.70	0.0332	−0.69	0.2759	−0.24	0.9655	0.66	0.7191
x_2x_3	1.82	0.1067	0.063	0.9158	1.70	0.7644	0.64	0.7284
x_1^2	−0.36	0.7245	2.70	0.0058	−1.93	0.7430	1.07	0.5794
x_2^2	2.13	0.0784	0.57	0.3726	10.74	0.1121	2.07	0.3030
x_3^2	3.87	0.0101	−3.43	0.0021	−3.55	0.5525	−0.54	0.7770

Table 5. Empirical models of responses in terms of actual factors

Empirical models	EQ no.	P-value	F-value	R^2	R^2_{adj}
ε=212.1172−0.5732O−24.2705I−6.1509F+0.2426OI −0.6165OF+0.6924IF−0.05746O^2+0.9448C^2+1.2647F^2	(6)	0.0025	18.42	0.97	0.92
θ=143.5041−9.3381O−4.7989I+7.5119F+0.0500OI −0.1571OF+0.0238IF+0.4316O^2+0.2546I^2−1.1190F^2	(7)	0.0026	18.34	0.97	0.91
T=450.4222−8.2520O−105.8791I+41.5139F+2.4550OI −0.0556OF+0.6457IF−0.3091O^2+4.7716I^2−1.1584F^2	(8)	0.0003	42.95	0.99	0.96
ST=257.4322−17.6970O−36.4078I+13.6187F+1.7206OI +0.1505OF+0.2421IF+0.1707O^2+0.9189I^2−0.1758F^2	(9)	0.0001	67.02	0.99	0.98

decreases, the quantity of the coefficient becomes larger.

Table 5 clearly shows that the P-value of all models is less than 0.05, which confirms the qualification of the obtained data. The calculated R^2-values are greater than 0.9 for all models indicating that more than 90% of the data deviation can be fitted by the empirical models. R^2_{adj} values of all models (in Table 5) are very close to R^2 values (greater than 0.9), which demonstrates agreement between models and data. The statistical significance of the second-order model equation was determined by F-value defined as a test for comparing the sources mean square to the residual mean square [57]. The F-value results imply that all models are significant and there is only 0.25%, 0.26%, 0.03%, and 0.01% chance for error due

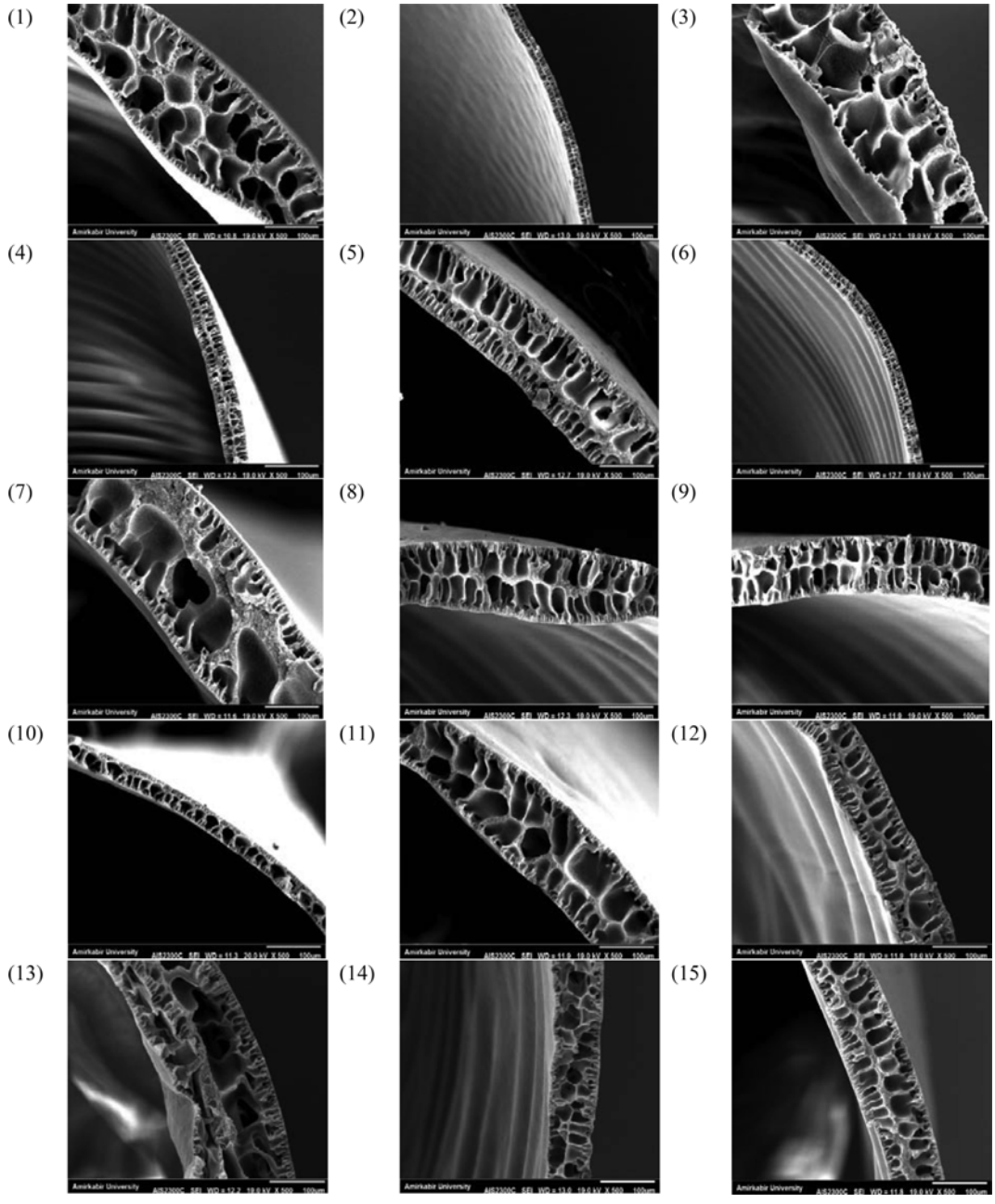

Fig. 3. Cross-section structure of dual-layer hollow fiber (experimental design tests).

to the noise of the porosity, contact angle, fiber thickness, and outer layer thickness responses, respectively.

1-2. Morphology of Hollow Fibers in DoE Tests

The SEM pictures of dual-layer hollow fiber membranes fabricated in DoE tests are shown in Fig. 3. Each image is separately shown in supplementary data (part S4) to clearly check the structure of the fibers. In general, the total structure of fibers is finger-like at both inner and outer layers due to immediate phase inversion induced by water in the internal and external coagulation. In fact, water is a strong coagulant for the polymer and the difference of solubility parameters of water and dope materials is high. Thus, it leads to an instantaneous de-mixing and fast precipitation rate, which is favorable for the formation of the membrane with a finger-like macro-voids structure [39,58]. As can be seen, in fibers 1, 3 and 13, by increasing the polymer concentration in the dope solution of outer layer with the same flow rate (4 ml/min), a long finger-like structure with large cavities changes to a shorter and smaller macro-voids like fiber 13. The structure of fiber 13 consists of two short finger-like structures near the inner and outer surfaces and a large finger-like between them. Similar cases could be detected for fibers 6, 2, 4 and 10, which were fabricated at 0.5 ml/min of dopes flow rate. In fiber 10, the finger-like structure almost disappeared and changed to the sponge-like structure in the outer layer. There is a thin sponge-like boundary between two finger-like structures of layers in fibers 5 and 7. This is because the polymer concentration in both inner and outer layer dope solution is

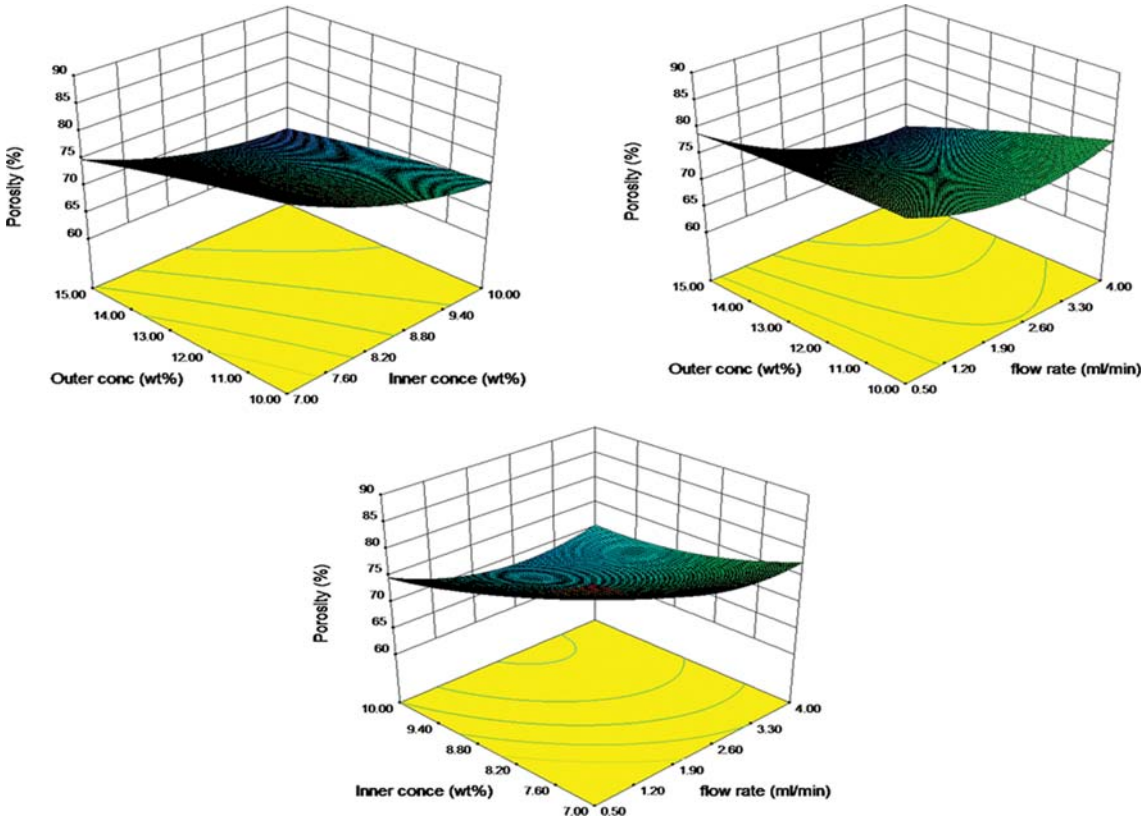

Fig. 4. Effect of the parameters on porosity.

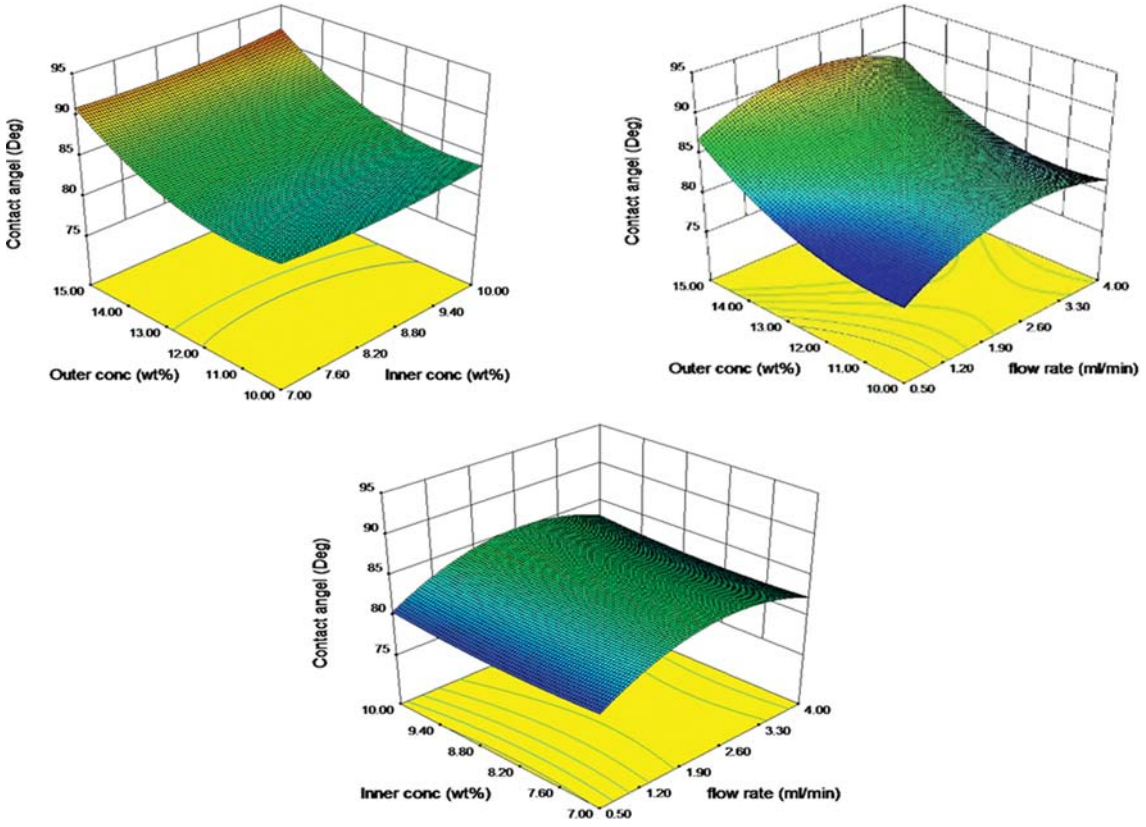

Fig. 5. Effect of the parameters on contact angle.

high and closed to each other. Experiments of 8, 12 and 15 were done under the same conditions (at the center points of each parameter), so their morphologies are similar. Fiber 9 has the same structures at the both of layers because the polymer concentration in each dope solution of layers was 10 wt%.

As a result, the morphology of the membrane was affected by the polymer concentration. In fact, by increasing the polymer concentration or viscosity of the dope solution, the large macro-voids of the finger-like structure become short and small and even change to the sponge-like structure.

1-3. Effect of the Parameters on the Porosity

As shown in Fig. 4, the porosity of the membrane decreases with the increase of the polymer concentration in the outer layer. It is well-known that by increasing the polymer concentration in dope solution, the porosity is affected and decreased because of the reduction of empty voids and pore size in the membrane matrix [59].

The similar results obtained for the case of polymer concentration in the inner layer. It can be seen that the polymer concentration of the inner layer exhibits more impressive parameter than that one on the porosity with the P-value of 0.0004 (Table 4). This implies that the more portions of the spaces and voids of the fiber were occupied by the inner layer. By increasing the dope flow rate, the porosity of membrane first decreases and then remains constant without obvious change, as well. This reveals that the increase in the dope flow rate can slightly decrease the pore size of the fibers.

1-4. Effect of the Parameters on the Contact Angle

The p-value of the polymer concentration in the outer layer is 0.002 for the hydrophobicity of the membrane (Table 4). This confirms that it is the most impressive parameter among the others. Fig. 5 indicates that the contact angle increases slightly by increasing of polymer concentration up to 12 wt%. Then, significant growth is observed from 84 to 91° when the polymer concentration varies from 12 to 15 wt%. This occurs due to the growth of hydrophobic polymer (PVDF) at the fiber surface. Fig. 5 also shows that the polymer concentration in the inner layer has no obvious influence on the contact angle. This verifies the significance of DoE results. The contact angle increased from 80 to 84° when the dope flow rate varied from 0.5 to 2.6 ml/min. Then, the contact angle decreased from 84 to 82° by increasing the flow rate over 2.6 ml/min. According to this result, no clear trend could be attained between the flow rate and the contact angle of the fiber. Furthermore, the variation of contact angle changing (80-84°) is not considerably affected by dopes flow rate.

1-5. Effect of the Parameters on the Membrane and Outer Layer Thickness

Fig. 6 and Fig. 7 demonstrate the effect of the parameters on the membrane thickness and the outer layer thickness, respectively. Both of the responses increase when the polymer concentration of the outer layer and dope solution viscosity increase. This result is in agreement with the observation of Wu et al. [60]. The same trend could be observed for membrane thickness when the polymer concentration in the inner layer increases. Based on ANOVA results (Table 4) the polymer concentration in the inner layer has P-values of 0.1810 via the thickness of the outer layer. This result makes

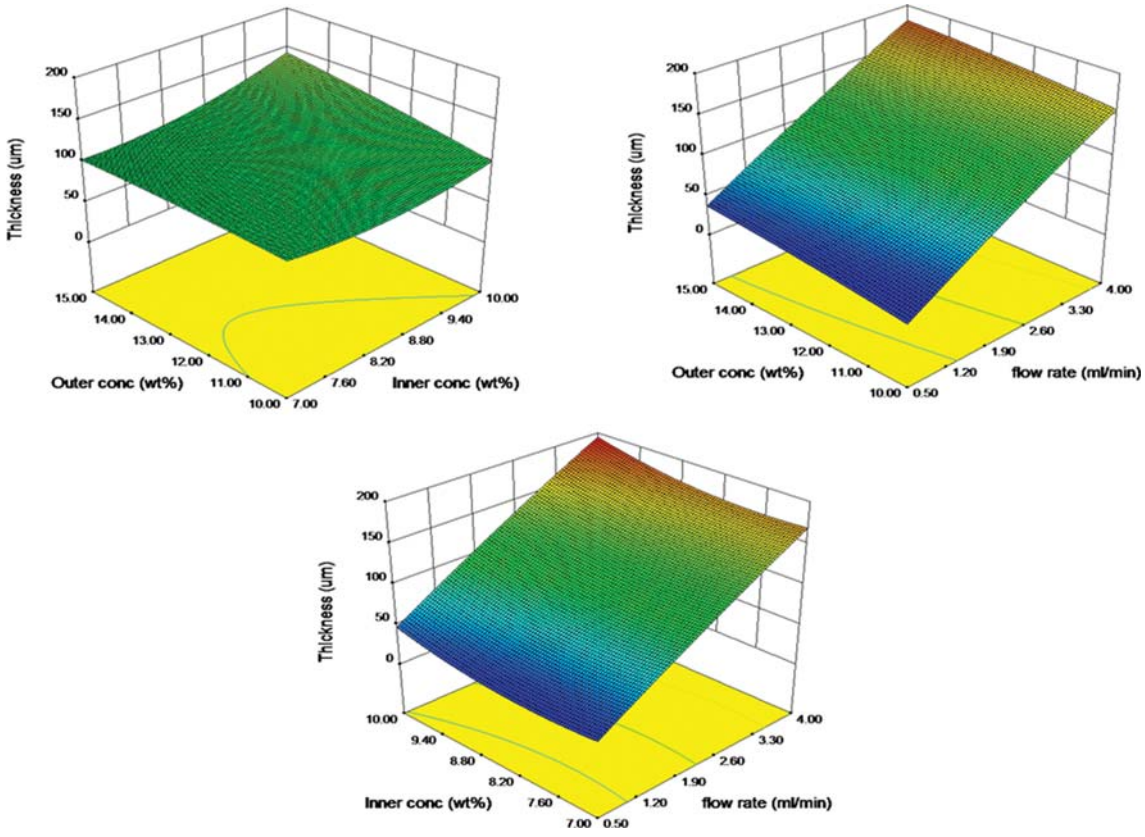

Fig. 6. Effect of the parameters on the membrane thickness.

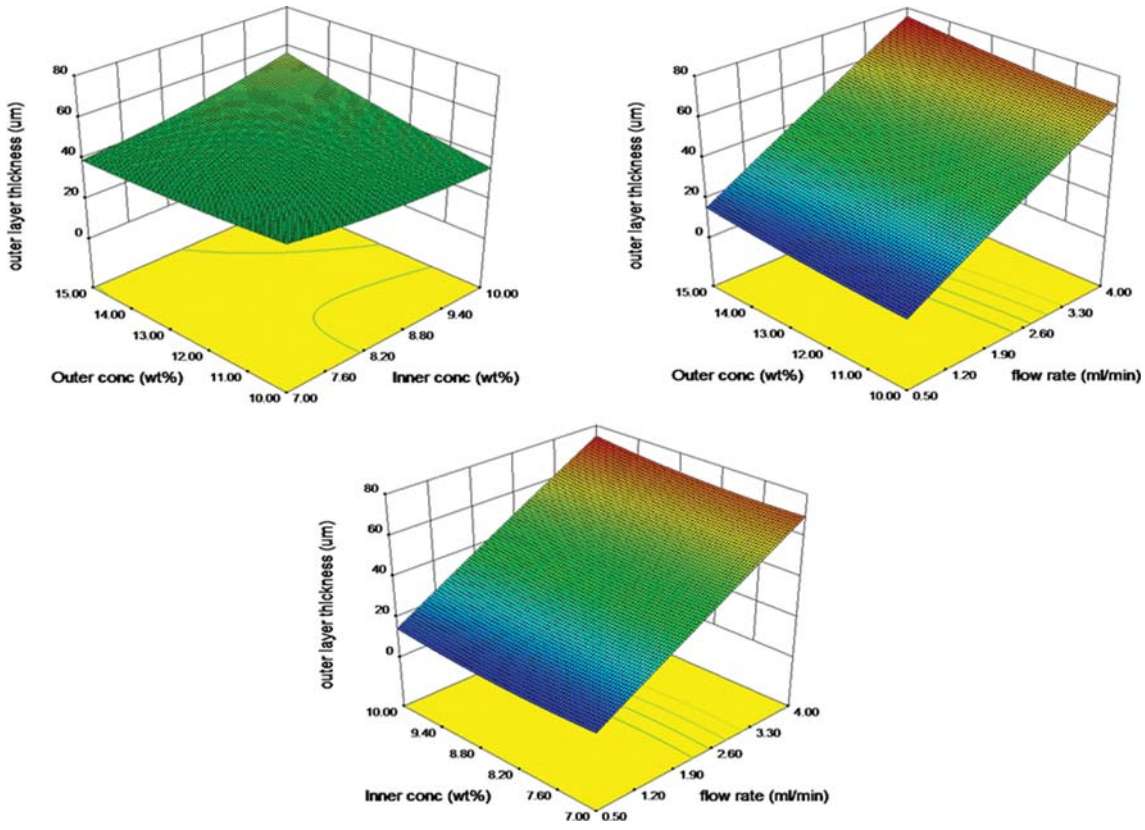

Fig. 7. Effect of the parameters on the outer layer thickness.

the proposed models more reliable. Chung et al. [61,62] found that a higher dope flow rate, which results in higher dope shear rate in the spinneret, forms a thicker and denser layer after the dope solution being extruded from the spinneret. It was observed that the molecular chains at higher shear rate tend to align themselves more than ones at lower shear rate due to the enhancement of molecular orientation which leads to a tighter structure. As a result, an increase of the dope flow rate strongly affects the fiber and outer layer thickness and make them thicker. Note that the dope flow rate has the most significant effect on the thickness and the outer layer thickness of fiber with the least P-value (<0.0001).

The one-factor and contour line plots of the parameters effect on the responses were illustrated by the software, as well. They could be found in supplementary data (part S5).

1-6. Optimization of the Parameters

After determining the effects and relations between parameters and their respective responses, the optimum values must be determined by the Box-Behnken method to reach an appropriate hollow fiber membrane. The number of responses is approximately high in this study. Hence, in order to optimize the parameters, we recommend that the responses become localized inside the valid regions. These regions were attained based on our observations and the recommendation of previous studies. The porosity and hydrophobicity should be as high as possible to increase the mass transport and wetting resistance of membrane during the MD process. In this regard, the values adopted for porosity and contact angle are more than 70% and 85°, respectively. It was observed that the fabricated fibers with the thickness of lower than 100 μm, have a weak mechanical resistance and quality. Therefore, the wall thickness chosen for the optimization of fibers is in the range of 100-200 μm. On the basis of modeling results reported by Lagana et al. [18] with consideration of mass and heat transport effects, an optimum thickness of the outer layer is about 30-60 μm. This range was accordingly considered for the optimization step in this study.

Finally, by taking into account all the valid regions of responses, the predicted point was suggested by the software is shown in Table 6. The results in optimization section have been shown in supplementary data (part S6).

Table 6. The predicted point by Box-Behnken in the optimization section

Parameters		Responses	
Polymer concentration in the outer layer (wt%)	13.49	Porosity (%)	74.98
Polymer concentration in the inner layer (wt%)	7.14	Contact angle (°)	86.24
Flow rate of dope solutions (ml/min)	2.99	Thickness of fiber (μm)	132.086
		Thickness of outer layer (μm)	52.871

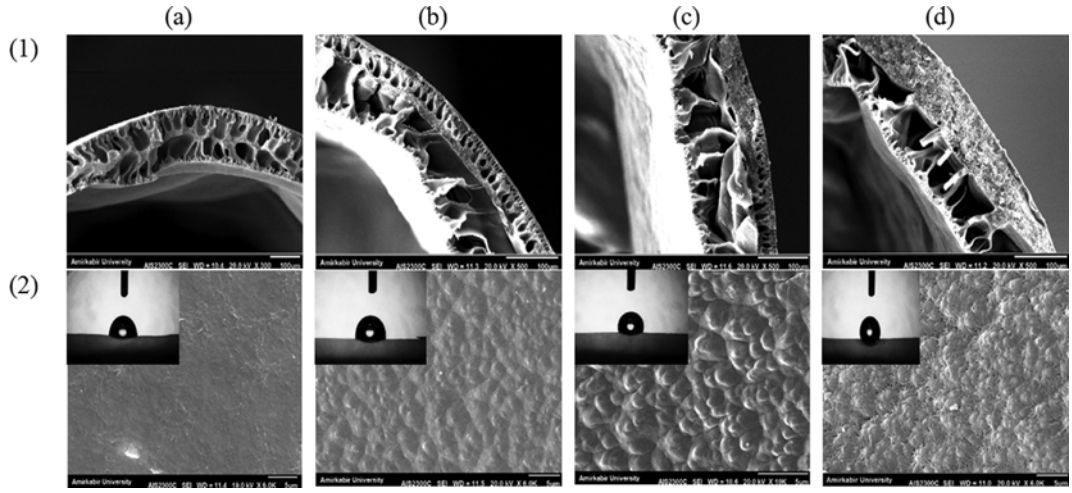

Fig. 8. Effect of different coagulation on the external hollow fiber morphology ((1) fiber cross sections; (2) fiber external surface and contact angel pictures); (a) water; (b) water/methanol (60/40, w/w); (c) water/methanol (40/60, w/w) and (d) water/methanol (20/80, w/w) used as the external coagulation in the coagulation bath.

2. Morphology Study

2-1. External Coagulant

Four hollow fibers were fabricated at the predicted point obtained by RSM method with different types of water/methanol compositions in the external coagulant. The other conditions were adjusted similarly to the DoE tests. Fig. 8 shows SEM pictures obtained from the cross-section and top surface of fibers. It can be observed that long finger-like macro-voids and cavities were formed in membrane structure when a strong non-solvent like water was used for coagulation (Fig. 8(1a)). By adding methanol, which is a weaker non-solvent for PVDF compared to water, the morphology of fiber changed from large finger-like to the short finger-like along with sponge-like structure (Fig. 8(b), (c)). By increasing the methanol percent in the coagulation bath, the growth of sponge-like structure can be clearly observed in the outer layer of fibers. In the case of water/methanol (20/80, w/w), the finger-like structure is completely disappeared and the morphology of the outer layer is fully dominated by the sponge-like structure (Fig. 8(1d)). The structure of the inner layer remains unchanged in all of the cases. It can be concluded that the type of the coagulation plays a significant role in the morphology of membranes prepared by phase inversion process. In general, a strong coagulant leads to a fast precipitation and solidification rate resulting in the long finger-like and large cavities formation, whereas a weak coagulant decreases precipitation rate and delays de-mixing process, which results in a porous sponge-like structure [58]. The coagulation rate could be explained based on the mutual diffusivity of solvent/non-solvent and the solubility parameters of polymer, water, and methanol reported by many authors elsewhere [37,39]. The difference between solubility parameters becomes high when water is used as the non-solvent, which favors to a fast precipitation and forms a finger-like macro-void structure. The addition of methanol in the coagulant delays the coagulation process and reduces the gap between parameters forms a porous sponge-like structure.

As can be observed in Fig. 8(2), the outer surface morphology of hollow fibers is changed by altering the water/methanol compositions. When pure water was employed as a coagulant (strong coagulant) the outer surface became dense and smooth (Fig. 8(2a)). As water/methanol composition was employed and consequently methanol portion increased in the coagulant, the roughness of outer surface increased. This may be attributed to the increase in size and the number of pores on the outer surface [37,63].

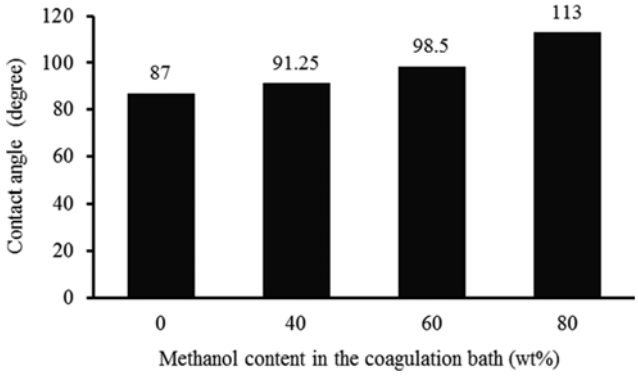

Fig. 9. Contact angle of outer fiber surface from different Methanol content in the coagulation bath.

Fig. 9 compares the contact angles of the outer surface in the different types of the coagulant. It can be clearly seen that the contact angle strongly depends on the coagulant compositions and accordingly increases when the roughness of surface increases. The spinning process became difficult when methanol content was 80 wt% in coagulant. In fact, this occurred due to the extremely slow precipitation and the deformation of the outer surface of the fibers during the spinning. Therefore, the mixture of water/methanol (40/60, w/w) was adopted as the standard composition in the external coagulation bath for the spinning process.

2-2. Internal Coagulant (Bore Fluid)

Fig. 10 shows four types of hollow fiber inner surface morphology prepared by different bore fluid compositions which contain water and solvent (NMP). The addition of the solvent into the bore

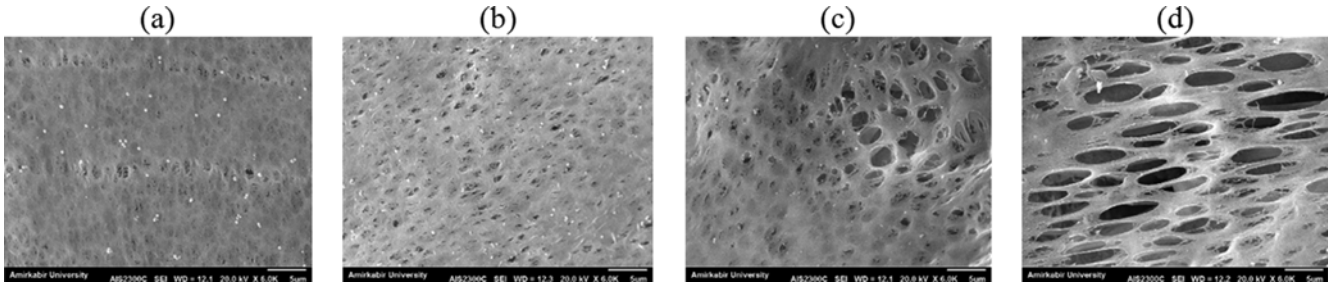

Fig. 10. Effect of different bore fluid compositions on the inner surface morphology of hollow fibers; (a) water, (b) water/NMP (90/10, w/w), (c) water/NMP (80/20, w/w), (d) water/NMP (70/30, w/w) used as the internal coagulation in the bore fluid.

fluid decreased the solubility difference (compared to pure water), and the precipitation rate in the lumen side was slowed down. This led to the formation of a porous inner layer surface and thus the mass transfer resistance on the inner side of hollow fiber decreased. It can be observed that the inner surface pores are larger than outer surface pores. This may be due to the inner side of fibers coagulated immediately after the extrusion of the dope solutions from the spinneret, while the outer side first passed through the air gap region and then coagulated. Khayet et al. [63] also found that the average nodule size of the inner surface was larger than that of the outer surface. The effect of the NMP on the pore size is highly significant for the evaluation of the inner surface structure. Hence,

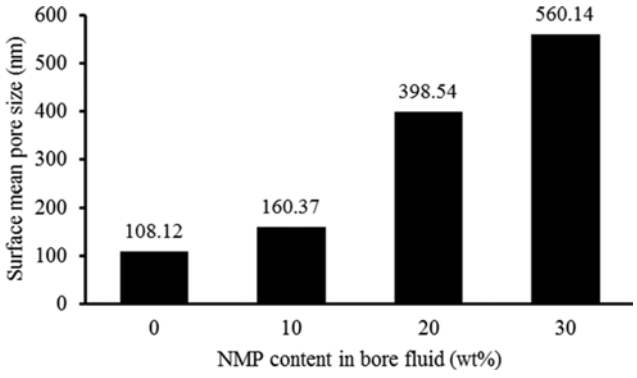

Fig. 11. Mean pore size of hollow fiber inner surface at the different NMP content in the bore fluid.

Fig. 11 demonstrates the effect of NMP content in the bore fluid on the mean pore size of inner layer surface calculated by Image-J software from the SEM pictures. The obtained results in this part are highly sophisticated and notable. It was found that the size of pores increased when the content of NMP in the bore fluid increased. During the spinning, the utilization of 70/30 wt% water/NMP as a bore fluid led to the deformation of the fiber. By considering the low polymer concentration in the inner layer dope solution, the high percentage of the solvent in the bore fluid could effectively diffuse to the inner skin and polymer matrix. Therefore, this weakened the substrate and thus, the size of pores at the surface became quite large (560.14 nm). As a result, a mixture of water/NMP (80/20, w/w) was applied as a standard bore fluid composition in the following section.

3. Fabrication of Resultant Dual-layer Hollow Fibers

Two hollow fibers were fabricated at different conditions obtained from each part. In the first part, an optimized fiber named HF-O was fabricated at the predicted point (Table 6) suggested by the Box-Behnken method. Then, a modified fiber named HF-M was fabricated at the standard conditions obtained by the combination of the optimized point, morphology study results and the utilization of EG as a non-solvent into the inner layer dope solution. EG is soluble in a mixture of water/NMP and leaves the membrane after spinning which results in pore formation and thus, enhances the membrane porosity [22,36]. The spinning conditions applied for the fabrication of each fiber are shown in Table 7.

3-1. Morphology of the Resultant Fibers

Fig. 12 displays the morphology of the resultant hollow fibers.

Table 7. Spinning conditions of the resultant dual-layer hollow fibers membranes

Membrane ID	HF-O	HF-M
Outer layer dope composition (wt%)	PVDF/NMP: 13.49/86.51	
Inner layer dope composition (wt%)	PVDF/NMP: 7.14/92.86	PVDF/EG/NMP: 7.14/6/86.86
Dopes flow rate (ml/min)	2.99	
Bore fluid (wt%)	ID water/NMP: 100/0	ID water/NMP: 80/20
Bore flow rate (ml/min)	6	
External coagulation (wt%)	ID water/methanol: 100/0	ID water/methanol: 40/60
Air gap (cm)	2	
Take-up speed	Free fall	

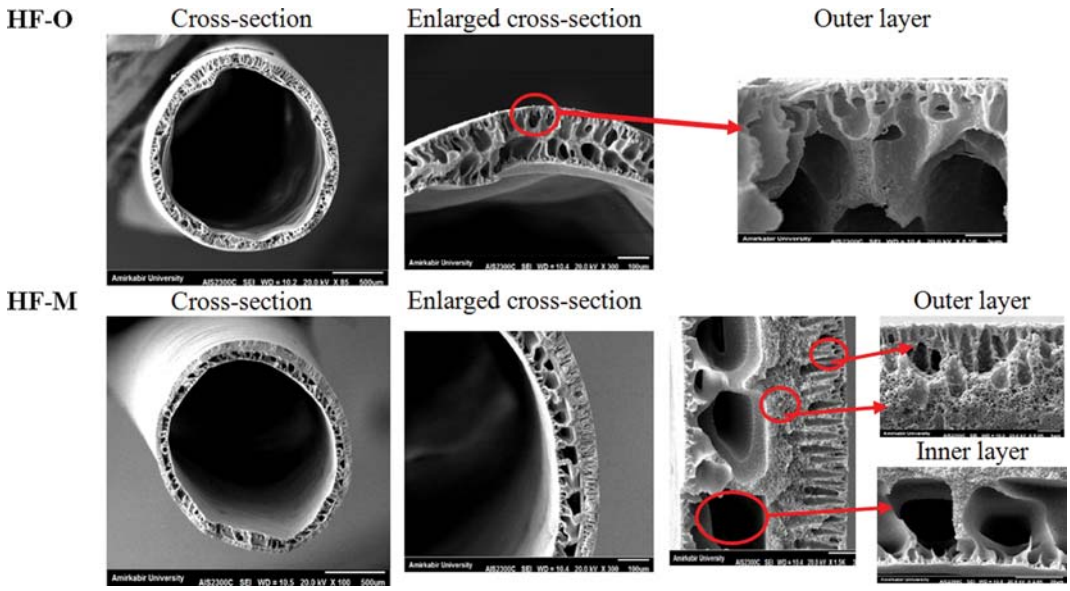

Fig. 12. SEM pictures of HF-O and HF-M hollow fiber membranes.

The surfaces (inner and outer surface) of the fibers (HF-O and HF-M) are shown in Fig. 8 and Fig. 10. Fig. 8(a) and Fig. 8(c) present the SEM images of the outer surface of HF-O and HF-M, respectively. Moreover, Fig. 10(a) and Fig. 10(c) demonstrate the SEM images of the inner surface of HF-O and HF-M, respectively. By comparing the cross-section of fibers (Fig. 12), the lumen side of HF-O is almost non-circular shape, whereas HF-M has a circular shape on the inner side. This is because the coagulation process is delayed by the presence of NMP into the bore fluid and allows the macromolecules enough time to relax and rearrange. Hence, the contour of the lumen side becomes regular and circular [51,64]. The morphology of each fiber is completely different. Indeed, the structure of HF-O is finger-like macro-voids in both layers and the size of pores in the inner layer is larger than the outer layer, which is due to the difference of polymer concentration in the dope solutions. Three types of structures could be seen in HF-M membrane. Fiber morphology near the inner layer is fully finger-like with large macro-voids and has a regular shape. The macro-voids of HF-M are larger than that of HF-O, which may be attributed to the presence of EG in the dope solution of HF-M membrane. The middle region is covered by the fully porous sponge-like structure. Generally, the coagulation in the middle region of fiber takes place later than the inner and outer region. This deaccelerating precipitation leads to the formation of sponge-like structure.

A thin and sharp finger-like with a sponge-like structure could be observed near the outer layer. The large macro-voids contain a high volume of air in the membrane, and consequently decrease the thermal conductivity and mass transport resistance. Therefore, the temperature profile remains constant between the streams and the permeation flux improves during DCMD test. However, macro-voids weaken the mechanical properties of the membrane and facilitate pore wetting [39,65,66]. It can be seen in Fig. 12 that the layers of both membranes have a good adhesion without any delamination, as well.

3-2. Characterization Results

The properties of HF-O and HF-M membranes obtained from the characterization tests are tabulated in Table 8. For HF-O, the values of porosity, contact angle, wall and outer layer thickness, which had been adopted as responses for DoE, are very similar to the values predicted by the proposed empirical models (Table 6). These results imply that the validation of the empirical models is high with the most accuracy. The obtained models in this work could be recommended as the main reference for the fabrication of the dual layer PVDF hollow fiber membranes for the future studies.

As indicated in Table 8, the porosity of HF-M has increased up to 87.32%. The utilization of EG as a non-solvent into the dope solution of the inner layer is the main reason for the increasing of the porosity. Moreover, increasing the pore size on the inner sur-

Table 8. Characterization properties of dual-layer hollow fibers

Fiber ID	Porosity (%)	Contact angle (°)	Wall thickness (μm)	Outer layer thickness (μm)	OD/ID (μm)	Gas permeation test: MPS, d_p (μm)	LEP (bar)	Strain at break (%)	Tensile stress at break (MPa)	Young's modulus (MPa)
HF-O	75.2±0.4	86±0.6	138.80±8	51.16±2	1818.41/ 1540.82	0.48±0.08	0.85±0.05	120.69±3	2.02±0.06	26.7±1.2
HF-M	87.3±0.6	98±1.0	131.14±8	54.30±2	1662.24/ 1399.98	0.4±0.06	1.3±0.1	137.22±2	2.23±0.08	29±0.8

face and the formation of porous sponge-like structure in the outer layer results in increasing the porosity of the fiber. The contact angle of HF-M is 12 degrees more than HF-O, which may be attributed to the usage of 60% of methanol in the external coagulation. In both cases, the thickness of the wall and the outer layer is approximately similar. This may be due to the same conditions such as dopes flow rate, and the polymer concentration of the inner and outer layer applied during the spinning process. As was expected, the thickness of the outer layer is in the range of 30-60 μm, which had been suggested by Lagana et al. [18]. The comparison of outer and inner layer diameter of membranes reveals that these values are smaller for HF-M rather than HF-O. This most probably corresponds to the coagulation process and the precipitation rate at the internal and external surfaces. In fact, by decreasing the precipitation rate (inducing solvent into the bore fluid and methanol into the external coagulation), the polymer chains have enough time to rearrange and release from the stresses generated by spinneret after extruding. Hence, the inner and outer diameter becomes smaller and more regular. A strong coagulant fluid like water causes immediate precipitation at the inner side of fiber after the dope solution being extruded from spinneret, which leads to bigger inner diameter and consequently outer one. These findings are one of the significant results obtained from this study.

The mean pore size (MPS, d_p) of dual-layer hollow fibers is related and controlled by the size of the pores in the outer layer. The results of gas permeation tests shown in Table 8 imply that this value for HF-O is more than HF-M owing to the structure of the outer layer; because other conditions have been the same for the fabrication of fibers. As a result, the mean pore size of the membrane is affected by the type of external coagulation and it is reduced when the structure of outer layer becomes porous sponge-like.

As shown in Table 8, the LEP_w of HF-O is less than HF-M membrane. LEP_w is one of the most important parameters in the membrane distillation and indicates the wetting resistance of membrane during the process. When the LEP_w increases, the wetting resistance improves, as well. It is known that the LEP_w highly depends on the pore size and hydrophobicity of the membrane [45]. This parameter is raised by the decreasing of the pore size and increasing of hydrophobicity.

In general, a sponge-like structure has a higher resistance to pore wetting than the finger-like macro-void structure [65]. All the mechanical properties of HF-M such as Young's modulus, stress, and strain at break are higher than HF-O. This is because of the presence of numerous large macro-voids and big cavities in both layers of HF-O which lead to the mechanical failure of the membrane. The stress-strain curve of both fibers could be found in supplementary data (part S7). Therefore, by comparing of characterization results between the resultant fibers, it can be concluded that HF-M has superior properties rather than HF-O.

4. DCMD Performance of Dual-layer Hollow Fibers

As presented in Fig. 13, the values of the permeation flux in the DCMD process are plotted versus feed inlet temperature. As expected, the vapor permeation flux almost exhibits exponentially dependence with the feed temperature and increases by raising this parameter. This may be due to the exponential relation between the vapor pressure and temperature of water according to the Antoine

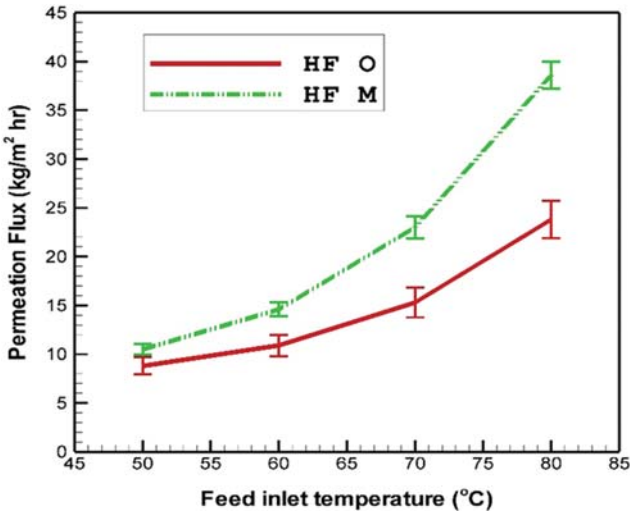

Fig. 13. Permeation flux of dual-layer hollow fibers vs feed inlet temperature.

equation [32,67]. All DCMD tests were conducted at the feed inlet velocity of 0.5 m/s and the permeate inlet velocity of 0.25 m/s, which flowed co-currently through the module. Moreover, the inlet temperature of the permeate stream was kept constantly around 20 °C. Although the structure of HF-O is macro-voids in both layers, which can reduce the mass transfer resistance across the membrane, the performance of HF-M is much better. This could be explained by following reasons: (1) the porosity of HF-M is 12.1% higher than HF-O, (2) the large macro-voids in the inner layer could enhance the driving force and consequently vapor permeation owing to smaller tortuosity and high porosity, (3) the big pores of inner surface made by inducing the solvent into the bore fluid, provide high liquid-vapor interfacial area which facilitates effective mass transfer across the membrane. In Fig. 13 the difference of permeation flux between fibers gradually increases by the growth of the feed temperature. This implies that the performance of membranes reveals further at the high temperature. The maximum flux of HF-M reaches as high as 38.6 kg m^{-2} hr^{-1} at the feed inlet tem-

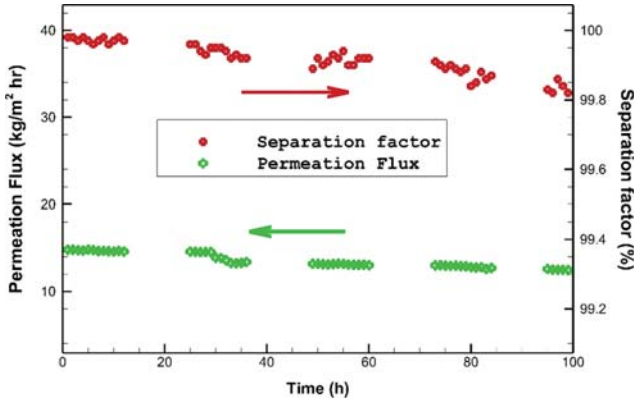

Fig. 14. The variation of permeation flux and separation factor during the long-term desalination performance (HF-M). Hot feed: 3.5 wt% of NaCl, 60 °C, 0.5 m/s cold distilled water: 20 °C, 0.25 m/s.

perature of 80 °C, while this value for the HF-O is 23.8 kg m^{-2} hr^{-1}. In the both cases, the conductivity of permeate solution is less than 15 μs cm^{-1}, which leads to the separation factor >99.95 according to Eq. (3).

5. Long-term Desalination Performance

As shown in Fig. 14, a long-time continuous DCMD test was carried out for HF-M membrane over a period of 100 hr. HF-M was selected for this purpose due to better wetting resistance and superior properties. During the long-time experiment, the inlet temperature of feed and permeate was maintained constant at 60 and 20 °C, respectively. To keep the salinity of hot feed aqueous solution (3.5% of NaCl), the amount of permeated vapor was transferred from permeate side into the feed tank. Fig. 14 clearly shows that the performance of the membrane is relatively stable, which is due to its sufficient resistance against the pore wetting. A slight decline of permeation flux (around 10%) occurs after 32 hr, while the separation factor remains higher than 99.8% through the entire experiment time. The reduction of permeation flux in long-term desalination is probably attributed to the partial membrane pore wetting. This phenomenon facilitates the temperature polarization along the membrane surfaces, suppresses the driving force and eventually leads to the reduction of MD process efficiency.

CONCLUSIONS

We applied RSM and morphology study to examine the fabrication of the hollow fiber in the DCMD process. In the first part of current work, 15 experiments were designed by the Box-Behnken method to investigate the effects of three main spinning parameters on four relative responses (the properties of the fibers) by significant quadratic models. By this approach, the optimized point of variables was predicted over the valid region of the responses. In the second part, the morphology of fibers (outer layer and inner layer surface) was studied and two resultant fibers were fabricated at the obtained conditions of each part. The following conclusions can be drawn from this study:

(1) On the basis of the responses' P-values, the effect of polymer concentration in the outer layer on membrane hydrophobicity is more than the dope flow rate. The thickness of fibers (both of wall and outer layer) is strongly affected by dope flow rate. In addition, the polymer concentration of the inner layer has the most effect on the porosity, as well.

(2) According to the ANOVA results, all empirical models are significant. For all of the models, P-values are less than 0.003 and both of R^2 and R^2_{adj} are more than 0.9. Therefore, they can be used for the prediction of respective responses for all PVDF dual-layer hollow fibers in the future studies.

(3) By incorporating methanol into the external coagulant, the morphology of the outer layer of fibers is strongly changed and tends to a fully sponge-like structure (at 80 wt% of methanol). The contact angle of fibers increases obviously from 88° to 113° when the content of methanol varies between 0-80 wt%.

(4) By altering the NMP percent of 0-30 wt% into the bore fluid, the mean pore size of the inner surface of the fibers increases in the vast region from 108.12 to 560.14 nm. Moreover, the presence of NMP into the bore fluid makes the shape of the lumen side more circular.

(5) By deaccelerating the precipitation rate and the coagulation process in both internal and external surface, the outer and inner diameter of the fiber decreases.

(6) The proper conditions for the modified membrane (HF-M) include the optimized point of DoE results, utilization of EG in the inner layer, 60 wt% of methanol and 20 wt% of NMP into the external and internal coagulation, respectively. The DCMD flux of HF-M reaches as high as 38.6 kg m^{-2} hr^{-1} (at the feed temperature of 80 °C), and it is approximately 62% more than HF-O which was fabricated only by DoE results.

(7) The modified fiber exhibits stable permeation flux and wetting resistance with high separation factor (>99.8%) through the long-term desalination process up to 100 hr.

SUPPORTING INFORMATION

Additional information as noted in the text. This information is available via the Internet at http://www.springer.com/chemistry/journal/11814.

REFERENCES

1. R. F. Service, *Desalination freshens up*, Science, New York (2006).
2. I. C. Escobar, *Sustainability Sci. Eng.*, **2**, 389 (2010).
3. K. W. Lawson and D. R. Lloyd, *J. Membr. Sci.*, **124**, 1 (1997).
4. G. Amy, N. Ghaffour and Z. Li, *Desalination*, **401**, 16 (2017).
5. Z. Ding, L. Liu and M. El-Bourawi, *Desalination*, **172**, 27 (2005).
6. E.Curcio and E. Drioli, *Sep. Purif. Reviews*, **34**, 35 (2005).
7. M. Khayet, *Adv. Colloid Interface Sci.*, **164**, 56 (2011).
8. D. González, J. Amigo and F. Suárez, *Renew. Sust. Energy Rev.*, **80**, 238 (2017).
9. A. K. An, J. Guo and E. Lee, *J. Membr. Sci.*, **525**, 57 (2017).
10. R. Schofield, A. Fane and C. Fell, *J. Membr. Sci.*, **33**, 299 (1987).
11. E. Karbasi, J. Karimi-Sabet and J. Mohammadi-Rovshandeh, *Chem. Eng. J.*, **322**, 667 (2017).
12. L. Eykens, K. De Sitter and C. Dotremont, *Sep. Purif. Technol.*, **182**, 36 (2017).
13. R. Moradi, S. M. Monfared and Y. Amini, *Korean J. Chem. Eng.*, **33**, 2160 (2016).
14. J. Zahirifar, J. Karimi-Sabet and M. A. Moosavian, *Desalination*, **428**, 227 (2018).
15. M. El-Bourawi, Z. Ding and R. Ma, *J. Membr. Sci.*, **285**, 4 (2006).
16. A. Khalifa, H. Ahmad and M. Antar, *Desalination*, **404**, 22 (2017).
17. A. Burgoyne and M. Vahdati, *Sep. Sci. Technol.*, **35**, 1257 (2000).
18. F. Laganà, G. Barbieri and E. Drioli, *J. Membr. Sci.*, **166**, 1 (2000).
19. B. Ashoor, S. Mansour and A. Giwa, *Desalination*, **398**, 222 (2016).
20. F. Suárez, S. W. Tyler and A. E. Childress, *Water Res.*, **44**, 4601 (2010).
21. P. Wang, M. M. Teoh and T. S. Chung, *Water Res.*, **45**, 5489 (2011).
22. K. Y. Wang, S. W. Foo and T. S. Chung, *Ind. Eng. Chem. Res.*, **48**, 4474 (2009).
23. J. Phattaranawik, R. Jiraratananon and A. Fane, *J. Membr. Sci.*, **215**, 75 (2003).
24. Z. Wang and S. Lin, *Water Res.*, **112**, 38 (2017).
25. M. M. Teoh, T. S. Chung and Y. S. Yeo, *Chem. Eng. J.*, **171**, 684

(2011).
26. M. Khayet and T. Matsuura, *Ind. Eng. Chem. Res.*, **40**, 5710 (2001).
27. M. Khayet, J. Mengual and T. Matsuura, *J. Membr. Sci.*, **252**, 101 (2005).
28. F. Liu, N. A. Hashim and Y. Liu, *J. Membr. Sci.*, **375**, 1 (2011).
29. R. Moradi, J. Karimi-Sabet and M. Shariaty-niassar, *Korean J. Chem. Eng.*, **33**, 2953 (2016).
30. K. Schneider, W. Holz and R. Wollbeck, *J. Membr. Sci.*, **39**, 25 (1998).
31. L. Song, B. Li and K. Sirkar, *Ind. Eng. Chem. Res.*, **46**, 2307 (2007).
32. X. Yang, R. Wang and L. Shi, *J. Membr. Sci.*, **369**, 437 (2011).
33. C. F. Wan, T. Yang and G. G. Lipscomb, *J. Membr. Sci.*, **538**, 96 (2017).
34. X. Li, Y. Mo and J. Li, *J. Membr. Sci.*, **528**, 187 (2017).
35. P. Van de Witte, P. J. Dijkstra and J. W. A. Van den berg, *J. Membr. Sci.*, **117**, 1 (1996).
36. K. Y. Wang, T. S. Chung and M. Gryta, *Chem. Eng. Sci.,* **63**, 2587 (2008).
37. S. Bonyadi and T. S. Chung, *J. Membr. Sci.*, **306**, 134 (2007).
38. F. Edwie and T. S. Chung, *J. Membr. Sci.*, **421**, 111 (2012).
39. F. Edwie, M. M. Teoh and T. S. Chung, *Chem. Eng. Sci.*, **68**, 567 (2012).
40. M. Su, M. M. Teoh and K. Y. Wang, *J. Membr. Sci.*, **364**, 278 (2010).
41. J. Zhu, L. Jiang and T. Matsuura, *Chem. Eng. Sci.*, **137**, 79 (2015).
42. J. Zuo, T. S. Chung and G. S. O'Brien, *J. Membr. Sci.,* **523**, 103 (2017).
43. X. Feng, L. Y. Jiang and T. Matsuura, *Desalination*, **401**, 53 (2017).
44. A. Dastbaz, J. Karimi-sabet and H. Ahadi, *Desalination*, **424**, 62 (2017).
45. M. Khayet and T. Matsuura, *Membrane distillation: principles and applications*, Elsevier (2011).
46. K. Ravikumar, K. Pakshirajan and T. Swaminathan, *Chem. Eng. J.*, **105**, 131 (2005).
47. M. Khayet, C. Cojocaru and M. D. C. García-Payo, *J. Membr. Sci.*, **35**, 234 (2010).
48. M. Khayet, C. Cojocaru and M. Essalhi, *Desalination*, **287**, 146 (2012).
49. Z. W. Song and L. Y. Jiang, *Chem. Eng. Sci.*, **101**, 130 (2013).
50. D. Cheng, W. Gong and N. Li, *Desalination*, **394**, 108 (2016).
51. L. Shi, R. Wang and Y. Cao, *J. Membr. Sci.*, **305**, 215 (2007).
52. J. S. Kwak, *Int. J. Machine Tools and Manufacture*, **45**, 327 (2005).
53. N. Aslan and Y. Cebeci, *Fuel*, **86**, 90 (2007).
54. A. Hadi, J. Karimi-Sabet and M. A. Moosavian, *J. Supercrit. Fluids*, **107**, 92 (2016).
55. M. A. Bezerra, R. E. Santelli and E. P. Oliveira, *Talanta*, **76**, 965 (2008).
56. A. Zaherzadeh, J. Karimi-Sabet and M. A. Moosavian, *J. Supercrit. Fluids*, **103**, 105 (2015).
57. P. Rana-Madaria, M. Nagarajan and C. Rajagopal, *Ind. Eng. Chem. Res.*, **44**, 6549 (2005).
58. S. Deshmukh and K. Li, *J. Membr. Sci.*, **150**, 75 (1998).
59. D. Wang, K. Li and W. Teo, *J. Membr. Sci.*, **163**, 211 (1999).
60. B. Wu, K. Li and W. Teo, *J. Appl. Polym. Sci.*, **106**, 1482 (2007).
61. J. Qin and T. S. Chung, *J. Membr. Sci.*, **157**, 35 (1999).
62. J. Qin, J. Gu and T. S. Chung, *J. Membr. Sci.*, **182**, 57 (2001).
63. M. Khayet, C. Y. Feng and K. C. Khulbe, *Desalination*, **148**, 321 (2002).
64. Y. Santoso, T. S. Chung and K. Y. Wang, *J. Membr. Sci.*, **282**, 383 (2006).
65. N. Peng, T. S. Chung and K. Y. Wang, *J. Membr. Sci.*, **318**, 363 (2008).
66. M. Gryta and M. Barancewicz, *J. Membr. Sci.*, **358**, 158 (2010).
67. S. Bonyadi and T. S. Chung, *J. Membr. Sci.*, **331**, 66 (2009).

Supporting Information

Optimization and modification of PVDF dual-layer hollow fiber membrane for direct contact membrane distillation; application of response surface methodology and morphology study

Mehdi Bahrami*, Javad Karimi-Sabet,†, Ali Hatamnejad*, Abolfazl Dastbaz*, and Mohammad Ali Moosavian***

*Department of Chemical Engineering, Faculty of Engineering, University of Tehran, Tehran, Iran
**NFCRS, Nuclear Science and Technology Research Institute, Tehran, Iran
(*Received 7 October 2017 • accepted 23 February 2018*)

S1.1. Spinning Process

The polymer solutions and bore fluid were transferred from their respective storages into the triple-orifice-spinneret by the syringe pumps. The extruded fibers were firstly traveled through a certain distance of air gap region and then immersed into the coagulation bath. Thereafter, the nascent fibers were passed through the water bath by means of three guiding wheels and pulled into a collecting reservoir by a wind-up drum at least for 5 days to remove residuals. During spinning, it has been attempted that the take-up velocity is approximately kept as same as free falling velocity to prevent stretching of the fibers. Therefore, only the gravity force induces to the nascent fibers among the external elongation stresses. The flow rate of dope solutions was varied from 0.5 ml/min to 4 ml/min (same flow rate was applied for inner and outer layer solutions) while the bore flow rate fixed at 6 ml/min. It is worth mentioning that an unstable flow of bore fluid came out from the spinneret when the bore flow rate was less than 6 ml/min (leads to the formation of non-uniform fiber) but a steady flow was observed at this flow rate.

S1.2. Spinning Apparatus

S2. LEP_w, MEAN PORE SIZE AND MECHANICAL STRENGTH MEASUREMENTS

S2.1. Liquid Entry Pressure of Water (LEP_w) Measurement

The LEP_w of the membrane is the pressure that must be applied to the distilled water before it penetrates into the dried pores of the membrane [1]. The value of LEP_w must be measured to determine the membrane wetting resistance in MD process. LEP_w depends on the pore size and hydrophobicity of membrane which increases by decreasing the pore size and increasing the surface hydrophobicity. In this study, the homemade set-up conducted for LEP_w measurement is schematically shown in Fig. 2. The procedure of LEP_w measurement has been explained by Khayet et al. elsewhere [2]. According to this procedure, a respective module with the effective length of 8 cm is connected to the distilled water container pressurized by nitrogen cylinder at room temperature and the pressure is monitored by a digital pressure gauge. First, the slight pressure (0.1 bar) was applied to the container for 5 minutes to ensure the pressure was applied to the whole of the fiber surface and there is no leakage. Then the pressure was increased stepwise (increment

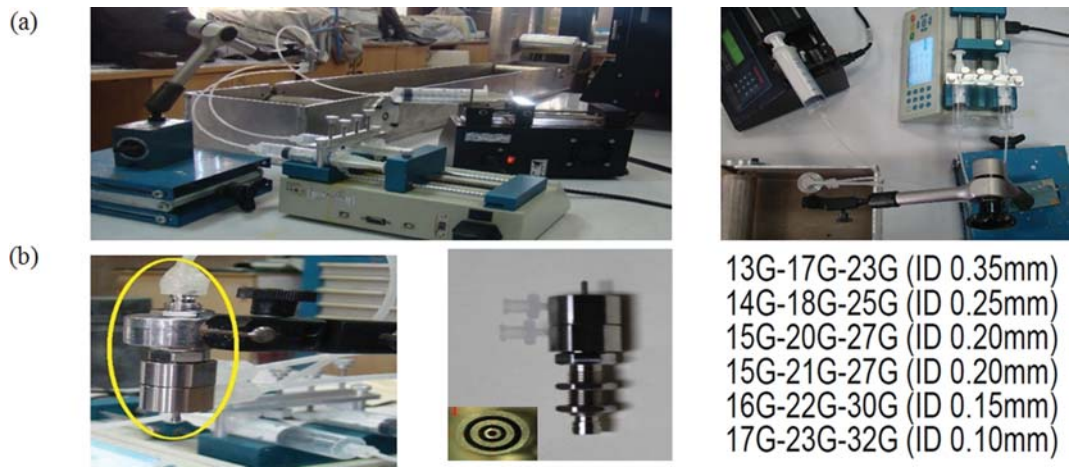

Fig. S1. (a) The spinning system and apparatus applied for the fabrication of hollow fibers, (b) the pictures and the dimensions of spinneret.

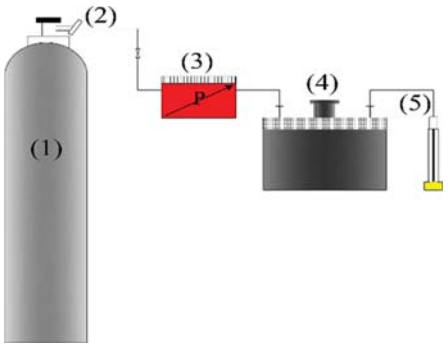

Fig. S2. The schematic of homemade set-up used for LEP_w measurement.
(1) Nitrogen cylinder
(2) Cylinder valve
(3) Pressure gauge
(4) Water container
(5) Hollow fiber module

of 0.05 bar) and kept at least for 5 minutes at each step. The pressure which at it the continuous flow of water was observed on the other side of the membrane is the LEP_w.

S2.2. Gas Permeation Test

The mean pore size (d_p) and the effective porosity (ε_e) of the membrane could be measured by gas permeation method. In this study, gas permeation test was used to determine the mean pore size of the membrane which is the important parameter in MD process. This procedure described by many authors [3-5] is as follows: (1) Nitrogen is pressurized through the membrane module with the effective length of 8 cm by a nitrogen cylinder and the pressure is monitored by a pressure gauge, (2) the gas is passed through the membrane and exit from the other side and its flow rate is measured by a soap bubble flow meter at room temperature. The schematic and real pictures of the gas permeation method are shown in Fig. 3. By considering that the pores structure in the skin layer of fiber is cylindrical and the gas flow through the membrane is a combination of Knudsen and Poiseuille flow, the gas permeance can be expressed as the following equation:

$$B_g = \frac{2}{3}\left(\frac{2}{\pi MRT}\right)^{0.5} d_p \varepsilon_e + \frac{P_m}{16\mu RT} d_p^2 \varepsilon_e = I_0 + S_0 P_m \quad (1)$$

Where B_g is the gas permeance (mol/m^2·s·Pa), M and μ are the molecular weight (g/mol) and viscosity (Pa·s) of nitrogen, respectively, R is the gas constant (Pa·m^3/mol·K) and T is the absolute

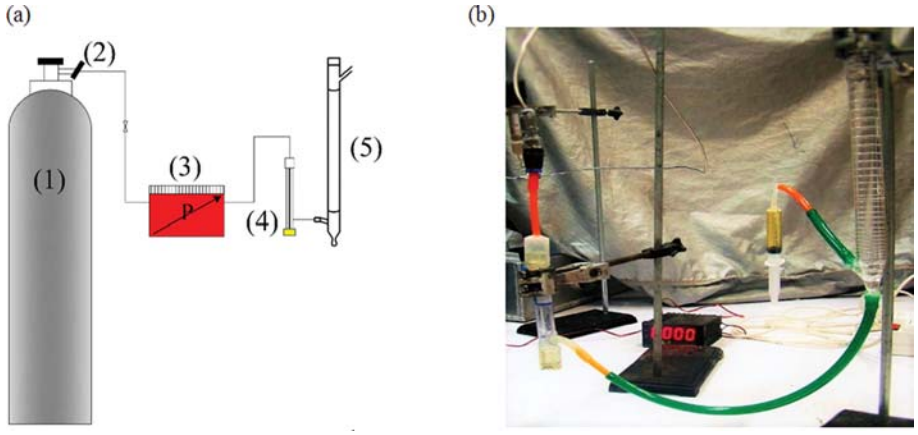

Fig. S3. Homemade set-up used for gas permeation method; (a) schematic picture and (b) real picture.
(1) Nitrogen cylinder (2) Cylinder valve (3) Pressure gauge (4) Hollow fiber module (5) Soup bubble flowmeter

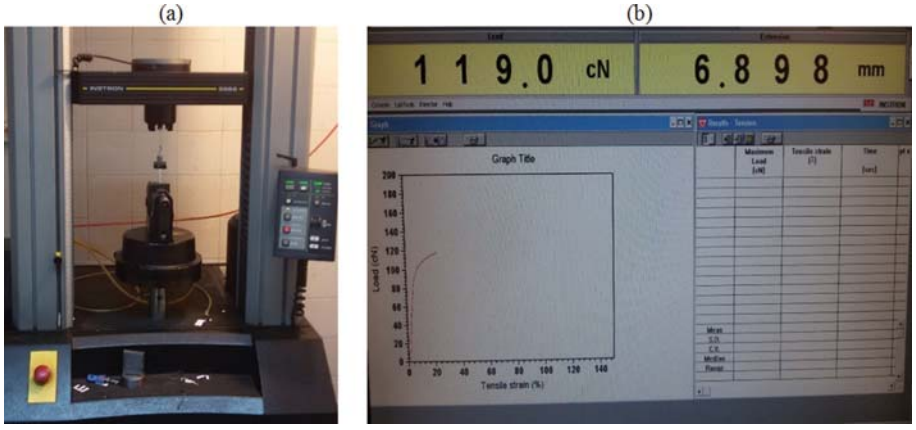

Fig. S4. (a) Instron tensiometer with the sample, (b) stress-strain curve monitored by computer.

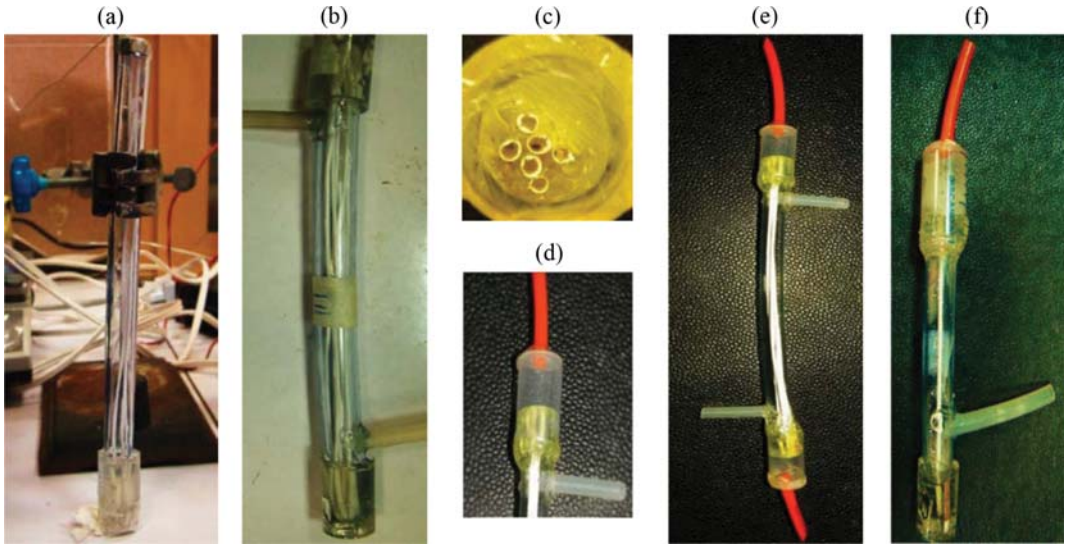

Fig. S5. The procedure of module fabrication.

temperature (K), P_m is the mean pressure (pa). By plotting linear dependence between B_g and P_m, the intercept (I_0) and the slope (S_0) can be determined and finally, the mean pore size can be calculated using the following equation:

$$d_p = \frac{32}{3}\left(\frac{S_0}{I_0}\right)\left(\frac{8RT}{\pi M}\right)^{0.5}\mu \quad (2)$$

S2.3. Mechanical Properties

The mechanical properties of hollow fiber in terms of Young's modulus (MPa), tensile stress at break (MPa) and strain at break (%) was measured using an Instron tensiometer (Sanwood technology Co., Guangdong, China) at room temperature. The sample with the effective length of 5 cm was clamped at both ends (Fig. 4(a)) and slowly pulled in tension with the elongation rate of 5 mm/min along the axial direction until the breakage occur. The mechanical properties of fibers could be obtained from the stress-strain curves drawn and recorded by computer software as shown in Fig. 4(b).

S3. MODULE FABRICATION

The module of the hollow fiber for DCMD has 6 fibers and for characterization tests has 1 fiber. To fabricate the module, first, the samples were cut and assembled into the plastic tube (inner diameter of 0.95 cm) and then both ends of the module were sealed by epoxy resin (Fig. 5(a) and (b)) to separate the shell and lumen side of the module. In the next step as shown in Fig. 5(d), two ends of module solidified were cut as the holes of fiber in the lumen side remain open and then the junctions were connected. Finally, the modules have been fabricated and ready to use in their respective applications (Fig. 5(e) and (f)). It is worth noting that only one ends of module prepared for characterization tests was cut and another one remain closed (Fig. 5(f)).

S4. THE SEM IMAGES OF THE RESULTANT FIBERS IN DESIGN OF EXPERIMENTS SECTION (FIG. 3)

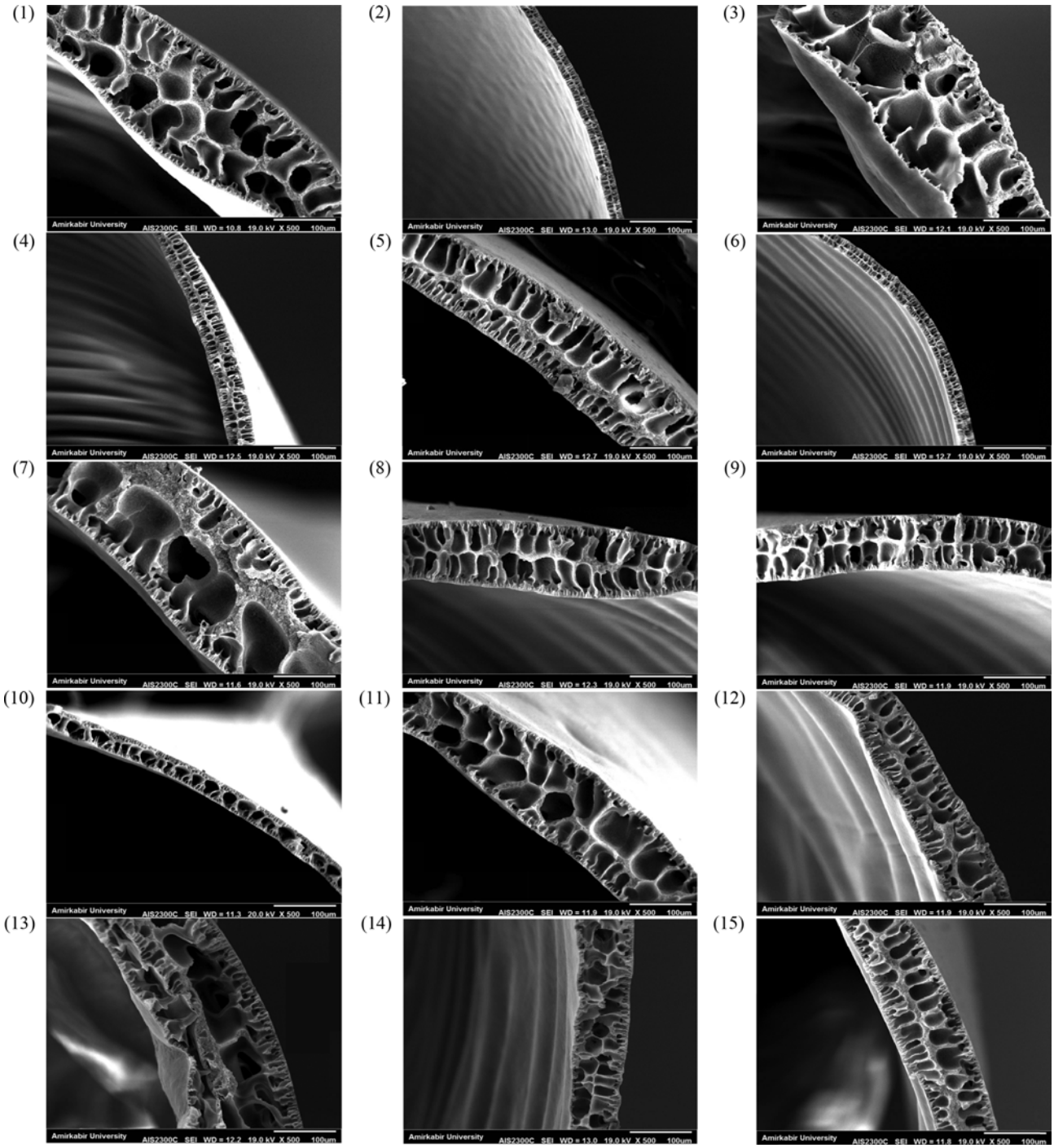

S5. THE ONE-FACTOR AND CONTOUR LINE PLOTS DESIGNED BY BOX-BEHNKEN

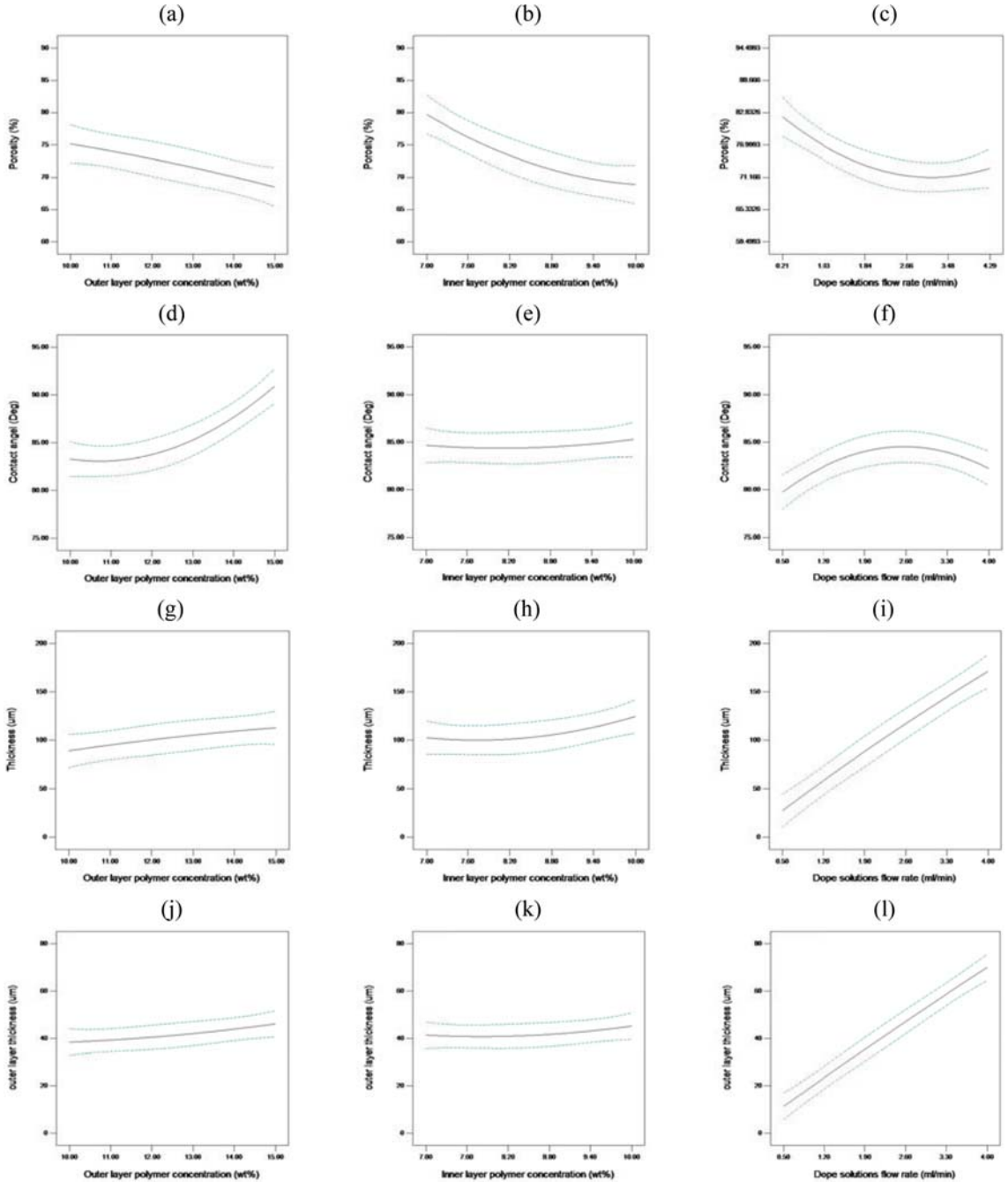

Fig. S6. The effect of the parameters on responses in one-factor plots.

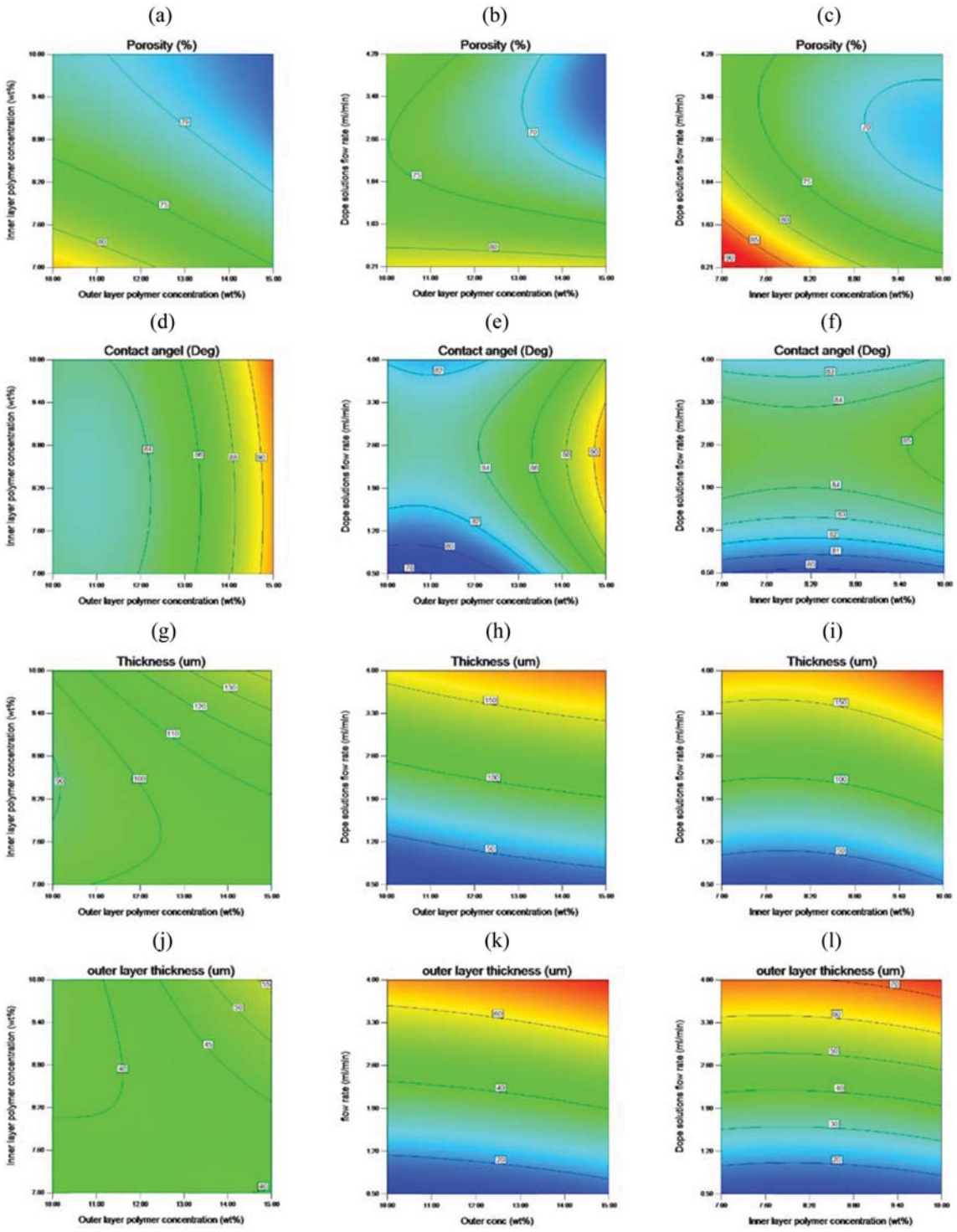

Fig. S7. The interaction effect of the parameters in the contour lines plots.

S6. PREDICTION OF BEST POINT

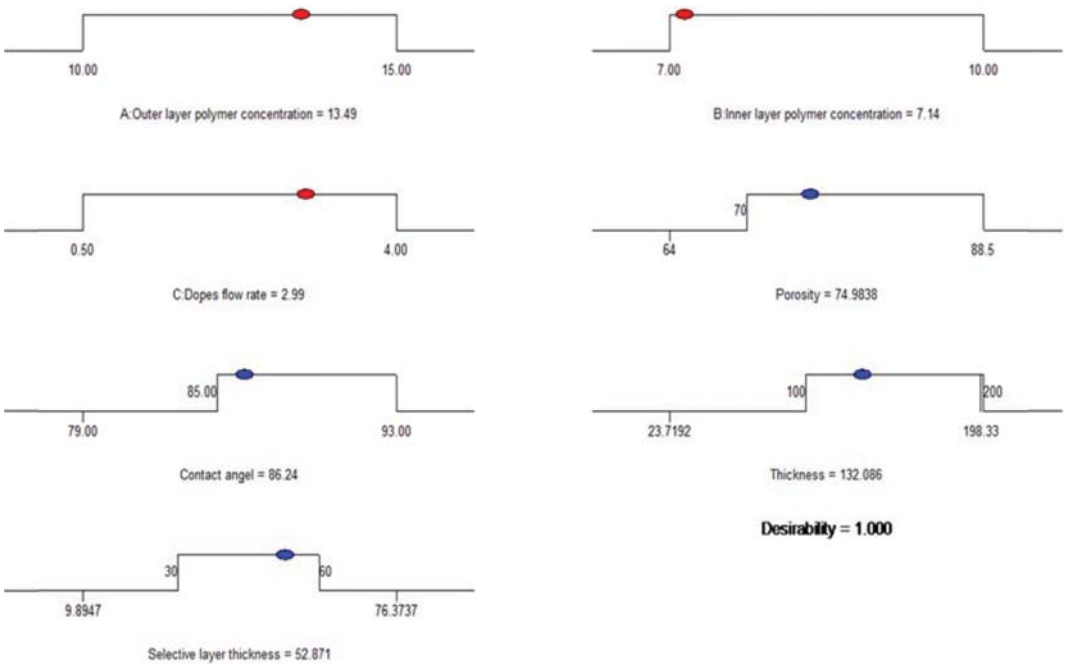

Fig. S8. The graph of the optimized point of the parameters and responses suggested by software.

S7. MECHANICAL PROPERTIES

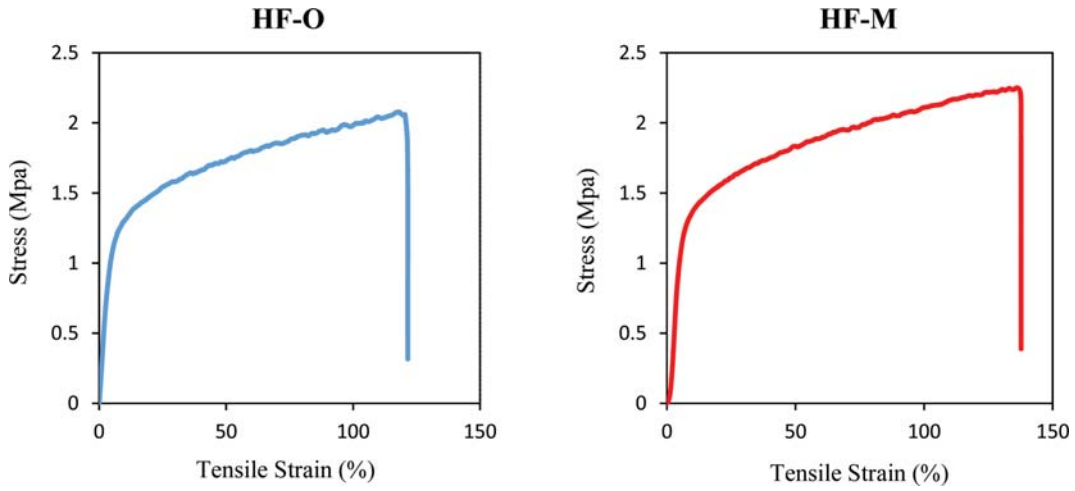

Fig. S9. Stress-strain curves for HF-O and HF-M dual-layer hollow fibers.

REFERENCES

1. M. Khayet and T. Matsuura, *Membrane distillation: Principles and applications*, Elsevier (2011).
2. M. Khayet, C. Y. Feng, K. C. Khulbe and T. Matsuura, *Polymer*, **43**, 3879 (2002).
3. K. Li, J. F. Kong, D. Wang and W. K. Teo, *AIChE J.*, **45**, 1211 (1999).
4. D. Wang, K. Li and W. K. Teo, *J. Membr. Sci.*, **163**, 211 (1999).
5. D. Wang, K. Li and W. K. Teo, *J. Membr. Sci.*, **178**, 13 (2000).